






# Natural Graphite Cuboids

Andrey V. Korsakov <sup>1,\*</sup>, Olga V. Rezvukhina <sup>1</sup>, John A. Jaszczak <sup>2</sup>, Dmitriy I. Rezvukhin <sup>1</sup>  
and Denis S. Mikhailenko <sup>1</sup>

<sup>1</sup> Sobolev Institute of Geology and Mineralogy, Siberian Branch of the Russian Academy of Sciences, 3 Koptyuga Avenue, 630090 Novosibirsk, Russia; olgashchepetova@igm.nsc.ru (O.V.R.); m.rezvukhin@igm.nsc.ru (D.I.R.); pazilovdenis@igm.nsc.ru (D.S.M.)

<sup>2</sup> Department of Physics and the A.E. Seaman Mineral Museum, Michigan Technological University, 1400 Townsend Drive, Houghton, MI 49931-1295, USA; jaszczak@mtu.edu

\* Correspondence: korsakov@igm.nsc.ru; Tel.: +7-383-333-2517

Received: 12 December 2018; Accepted: 5 February 2019; Published: 14 February 2019



**Abstract:** Graphite cuboids are abundant in ultrahigh-pressure metamorphic rocks and are generally interpreted as products of partial or complete graphitization of pre-existing diamonds. The understanding of the graphite cuboid structure and its formation mechanisms is still very limited compared to nanotubes, cones, and other carbon morphologies. This paper is devoted to the natural occurrences of graphite cuboids in several metamorphic and magmatic rocks, including diamondiferous metamorphic assemblages. The studied cuboids are polycrystalline aggregates composed either of numerous smaller graphite cuboids with smooth surfaces or graphite flakes radiating from a common center. Silicates, oxides, and sulphides are abundant in all the samples studied, testifying that the presence of oxygen, sulfur, or sulphides in natural systems does not prevent the spherulitic growth of graphite. The surface topography and internal morphology of graphite cuboids combined with petrological data suggest that graphite cuboids originated from a magmatic or metamorphic fluid/melt and do not represent products of diamond-graphite transformation processes, even in diamond-bearing rocks.

**Keywords:** graphite cuboid; diamond; cliftonite; sulphide

## 1. Introduction

Graphite, diamond, and lonsdaleite are well-known carbon polymorphs. The first two have broad industrial applications, while polycrystalline diamond-lonsdaleite aggregates are currently considered as a new super-hard material. Carbon polymorphs are of particular importance in the geosciences due to their inert and refractory nature. Moreover, diamond, graphite, and lonsdaleite are important PT-indicator minerals, with their stability fields defining lower pressure and temperature limits of host rocks.

There are numerous works devoted to the structure peculiarities and formation mechanisms of graphite, diamond, and lonsdaleite (see the review in [1]). The coexistence of the three carbon polymorphs was suggested in zircon-hosted microinclusions in garnet-biotite feldspathic gneisses from the Kokchetav massif [2]. The predominant model for the lonsdaleite formation assumes its crystallization under the shock-PT conditions characteristic of meteorites or impactites [3–13]. Such PT conditions are also probable in mantle environments. However, only controversial findings of lonsdaleite have been reported in eclogites from the Kola Peninsula [14], glaucophane-bearing eclogites of the Maksyutov complex [15], and garnet-biotite gneiss from the Kokchetav massif [16]. In contrast to lonsdaleite, which is always found as aggregates with other carbon polymorphs [17], diamond and graphite commonly occur separately, although in some localities, these carbon polymorphs can be recognized in an intimate association, as well (see [18] and the references therein). According to [19], most diamonds nucleated

heterogeneously on mineral seeds (e.g., sulphide, native iron, wustite, monocrystalline graphite), which could lower the energy barrier to nucleation of monocrystals. Alternatively, monocrystalline graphite inclusions [20] have been interpreted as the primary phases that were overgrown by diamond [21], whereas syngenetic growth of diamond and graphite has been proposed for the Kokchetav massif [22] and eclogitic xenoliths from the Udachnaya kimberlite pipe [18]. Graphite is a common accessory mineral in ultrahigh-pressure metamorphic (UHPM) rocks [23,24], which along with kimberlites, lamproites, and related mantle-derived rocks, are the primary source of terrestrial diamond. Graphite occurrences have also been documented in magmatic [25,26] and hydrothermal rocks [27–30].

In accordance with its symmetry and structure, graphite typically forms euhedral, tabular hexagonal crystals [31–33]. However, occasionally, graphite exhibits some exotic morphologies (e.g., tube, cone, fiber) resulting from distortions in the graphene sheets during growth, as well as from the incorporation of various defects such as dislocations, disclinations, twin planes, and pentagonal and heptagonal rings [34]. For instance, Jaszczak et al. [34] reported the spherical, spheroidal, conoid, and “triskelial” graphite aggregates in calcite boudins (Ontario, Canada), which were supposed to crystallize from metamorphic fluids. In general, diamond and graphite can be easily distinguished by morphology, but in some cases, graphite shows morphological features typical of diamond crystals, such as octahedrons and cuboids. Graphite octahedrons were described in garnet clinopyroxenites from the Beni Bousera complex [35,36], while graphite cuboids are particularly abundant in diamondiferous garnet-clinopyroxene rocks from the Kokchetav massif (Northern Kazakhstan) [22,37,38]. Graphite cuboids in metamorphic rocks have been interpreted as products of partial or complete diamond graphitization and thus as indicators of deep-seated (>120 km) origin of the host rocks [39–45]. Graphite cuboids and octahedrons (cliftonite; Figure 1) associated with native iron, which were initially considered to be pseudomorphs after diamond as well, are well-known in meteorites [46,47] and some terrestrial rocks (see [25] and the references therein).

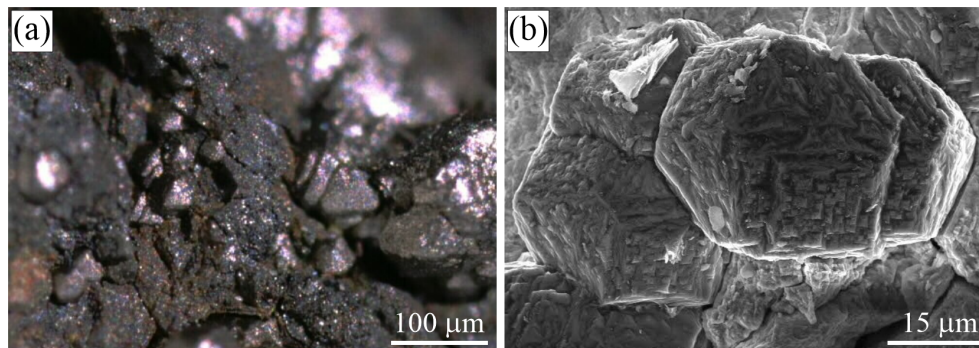


**Figure 1.** (a) Optical image showing cliftonite octahedrons in the Campo del Cielo iron meteorite, Chaco, Argentina, and (b) SEM secondary electron (SE) image of cliftonite from the Canyon Diablo iron meteorite, Meteor Crater area, Winslow, Coconino Co., Arizona, USA (samples from J.A. Jaszczak’s collection).

Two series of experiments, one “dry” and one “wet”, were performed in order to test the hypothesis of graphite cuboid formation due to diamond graphitization [48]. This experimental study revealed that in the “dry”-system at 2–2.5 GPa and 1400–2100 °C, even very fine details of the original cuboid and octahedron diamond crystals can be recognized on graphitized diamonds. In the “wet” system, none of the graphite cuboids, octahedrons, or complete graphite coatings on the original diamond crystals were observed (Figure 4 in [48]); however, similar to the results obtained in [49,50], many small negatively-oriented trigons were identified on the diamond {111} surfaces, testifying to their dissolution in H<sub>2</sub>O-rich fluid. Experimental studies of diamond and graphite crystallization from COH fluid or carbonate melt have demonstrated that at temperatures below 1300 °C, graphite is the first carbon polymorph to crystallize, even in the diamond stability field [51,52]. It should be noted that in all experimental runs, graphite appeared either as perfect hexagonal crystals [51] or



as a quenched soot, whereas graphite cuboids were never recognized. The conducted experimental studies clearly show that graphite cuboids can be obtained by diamond graphitization only in a “dry” system and at temperatures significantly higher than those reported even for ultrahigh-temperature complexes [53,54] and diamond-bearing metamorphic terrains [55–58]. Thus, the origin of graphite cuboids in natural systems remains poorly understood.

This study was undertaken to provide a mineralogical characterization of natural graphite cuboids from a series of worldwide terrestrial complexes with different geodynamic histories, i.e., the Kokchetav massif (Northern Kazakhstan), the Estes Quarry (West Baldwin, Cumberland County, ME, USA), the Maksyutov complex (South Urals, Russia), the Beni Bousera (Northern Morocco), and the Ozeraya mountain intrusion (Norilsk, Russia), as well as to address the question of graphite-cuboid genesis in the studied metamorphic and magmatic mineral associations.

## 2. Materials and Methods

In this study, graphite cuboids (2–1000  $\mu\text{m}$ ) were extracted by a thermo-chemical dissolution technique (the detailed description can be found elsewhere [59]). Extracted graphite grains, polished samples, and thin sections were studied at Sobolev Institute of Geology and Mineralogy, Siberian Branch of the Russian Academy of Sciences (Analytical Center for multi-elemental and isotope research SB RAS), Novosibirsk, Russia. The samples were examined in reflected polarized light using an Olympus BX-52 optical microscope. The compositions, secondary electron (SE), and back-scattered electron (BSE) images of minerals were acquired using a Tescan MIRA 3 LMU scanning electron microscope (SEM) coupled with an INCA Energy 450+ XMax 80 EDS system (Oxford Instruments, Oxford, UK). Analyses were carried out using an accelerating voltage of 20 keV, a beam current of 1 nA, and a beam size of 10 nm.

Raman spectra were collected using a Jobin-Yvon LabRAM HR800 Raman Spectrometer. The system was equipped with a frequency-doubled Nd:YAG laser emitting at 532 nm and an Olympus BX41 optical microscope with an Olympus MPlan 100  $\times$  /0.90 $\infty$ /0/FN22 objective. Spectra were collected at room temperature in backscattering geometry with a laser power of about 5 mW (to avoid graphite damage) and a spectral resolution of approximately 2  $\text{cm}^{-1}$ . Spectra were calibrated using the 520.6  $\text{cm}^{-1}$  line of a silicon wafer.

Carbon isotope compositions were determined on a Thermo Finnigan Delta Plus XL instrument. Analytical details of this procedure have been reported elsewhere [60].

## 3. Geological Settings and Sample Descriptions

A brief petrological summary for the studied rocks containing graphite cuboids is presented in Table 1. Mineral abbreviations used in Table 1 and throughout the text are as follows: Grt = garnet, K-Cpx = K-bearing clinopyroxene, Dol = dolomite, Cal = calcite, Mg-Cal = magnesian calcite, Bt = biotite, Ms = muscovite, Amp = amphibole, Kfs = K-feldspar, Qz = quartz, Tur = tourmaline, Czo = clinozoisite, Phe = phengite, Omp = omphacite, Gln = glaucophane, Ab = albite, Opx = orthopyroxene, Pl = plagioclase, Pgt = pigeonite, Wus = wustite, Tae = taenite, Ilm = ilmenite, Sul = sulphides, Po = pyrrhotite, Py = pyrite, Rt = rutile, Chl = chlorite, Zrn = zircon, Gth = goethite, Dia = diamond, Gr = graphite.

**Table 1.** Sample locations, mineral assemblages and graphite morphology. Graphite morphology: c = cuboids, s = spherulites, f = flakes, i.a. = irregular aggregates.

Location	Mineral Assemblages	Gr Morphology	Gr Size	PT
Kokchetav massif (Kazakhstan)	Grt + K-Cpx ± Dol ± Mg-Cal ± Sul	c, s, f	up to 700 µm	1000–1100 °C, 6–7 GPa [58]
	Grt + Bt + Kfs + Qz ± Ky ± Tur ± Czo ± Sul	c, s, f	up to 500 µm	950–1000 °C, 4–5 GPa [61]
Estes Quarry, West Baldwin, Maine (USA)	Ab	c, s, f	up to 1 mm	unknown
Maksyutov complex (South Ural, Russia)	Qz + Phe + Omp + Gln ± Sul	c, s, f	up to 15 mm	600 °C, 1.5–1.7 GPa [62]
Beni Bousera (Morocco)	Opx + Grt ± Sul	i.a., f	up to 15 mm	1300 °C, >4 GPa [63]
Ozernaya (Norilsk, Russia)	Fe <sup>0</sup> + Wus + Tae + Ilm + Pl + Pgt ± Sul	c	up 300 µm	750–1200 °C [25]

### 3.1. Kokchetav Massif

The UHPM rocks of the Kokchetav massif (Northern Kazakhstan) are the type locality of metamorphic diamonds [64–67]. However, as shown by De Corte et al. [68], the presence of graphite, fluid/melt, and carbonates is a prerequisite for diamond formation in these rocks. There are several diamond-bearing localities within the Kokchetav massif, with the Kumdy-Kol microdiamond deposits [40,41,65,66,69–72] and the Barchi-Kol area being the most renowned [61,73–80]. Graphite from these localities appears as nice euhedral flakes and their intergrowths, spherulites, and cuboids (Figures 2–7).

#### 3.1.1. Garnet-Clinopyroxene Rocks and Marbles

Garnet-clinopyroxene rocks and marbles have the highest diamond grade among the Kokchetav rocks and consist of variable amounts of garnet, clinopyroxene, phlogopite, and carbonates (dolomite or Mg-calcite) [41,67,71,81]. The diamond distribution in the garnet-clinopyroxene rocks from the Kumdy-Kol deposits is highly heterogeneous (Figure 2), and locally, the diamond contents reach 5000 carats per ton. Diamond crystals in these rock types may exceed 700 µm, while their average size is about 50 µm (Figure 2). There are yellowish or greenish diamond cuboids with well-defined growth zones [76,82–84]. Diamond crystals are often surrounded by graphite coatings of variable thickness. Graphite in this rock type occurs chiefly as spherulites or cuboids (Figure 6 in [22] and Figure 3). Single euhedral graphite crystals can be found exclusively as inclusions in diamond, K-bearing clinopyroxene, and garnet (Figure 5 in [22]).

In one sample of the garnet-clinopyroxene rock, there are several distinct zones characterized by a variable diamond and graphite content (Figure 2). Zone I contains the largest diamond cuboids up to 800 µm across. Graphite coatings on diamond crystals appear only occasionally within this zone. Zone II is enriched in sulphides (pyrrhotite, pyrite, chalcopyrite) and smaller diamond cuboids (up to 200 µm). These diamond grains are predominantly pure diamond crystals lacking graphite coatings and occur as inclusions in clinopyroxene and garnet or in the matrix. Note that diamond has been identified as inclusions in pyrrhotite from the Kumdy-Kol deposit for the first time (Figure 2a). Previously, Schertl et al. [85] and Mikhno and Korsakov [86] claimed that samples enriched in sulphides are diamond-free. Zone III is enriched in graphite cuboids, with some of these cuboids containing a diamond core. Within the sample, there are no regularities in the spatial distribution of pure diamond crystals and those with graphite coatings.

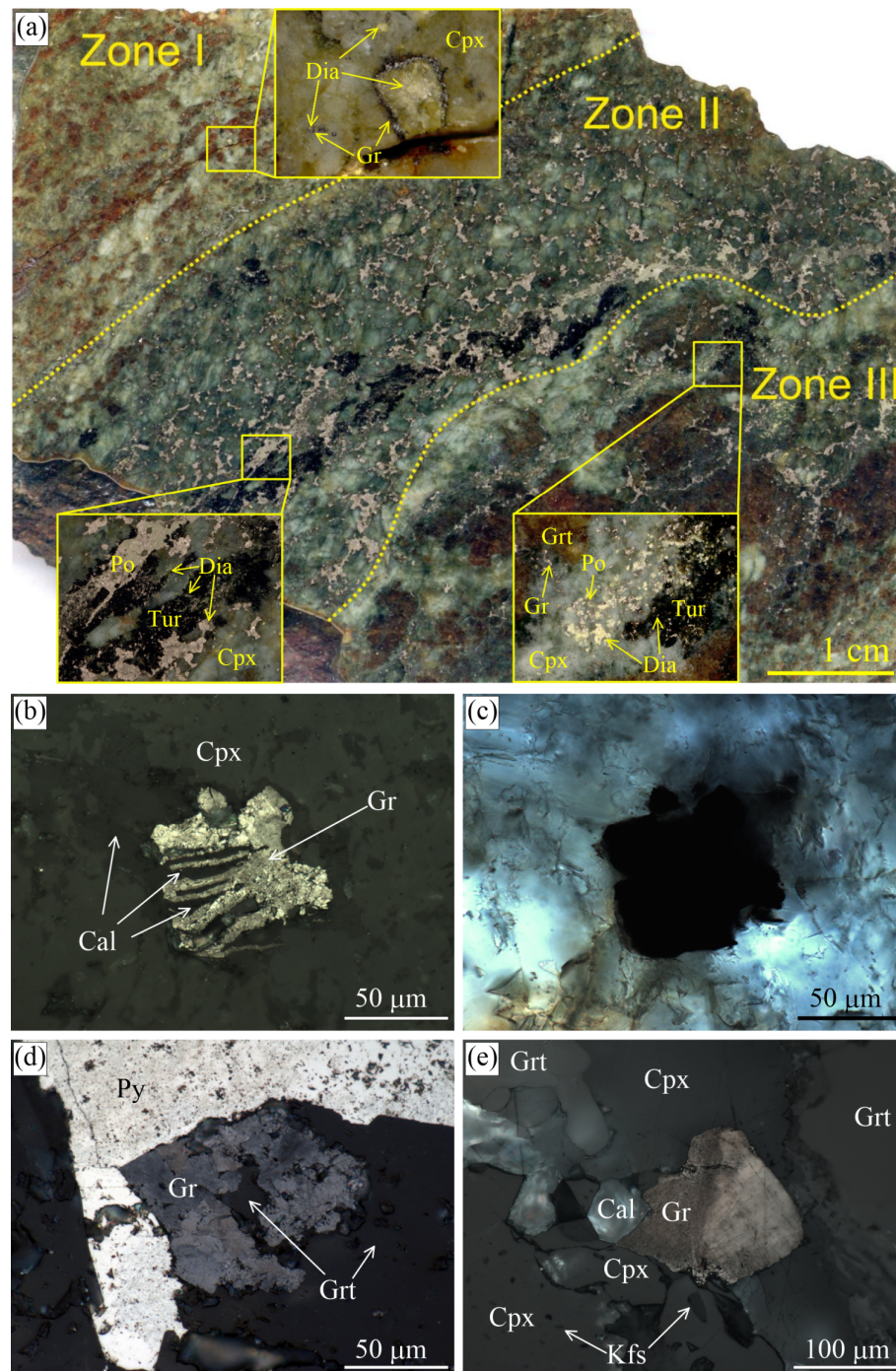


**Figure 2.** (a) Scanned fragment of the garnet-clinopyroxene rocks (Sample O24-4.5m-2018) from the Kumdy-Kol microdiamond deposit with marked zones of different diamond and graphite contents. Reflected (b,d,e) and transmitted (c) light images showing the internal morphology of different graphite cuboids from this sample. Some graphite cuboids that look like a massive aggregate in transmitted light (c) are actually very openwork and contain rock-forming minerals (b). Images (b) and (c) depict the same field.



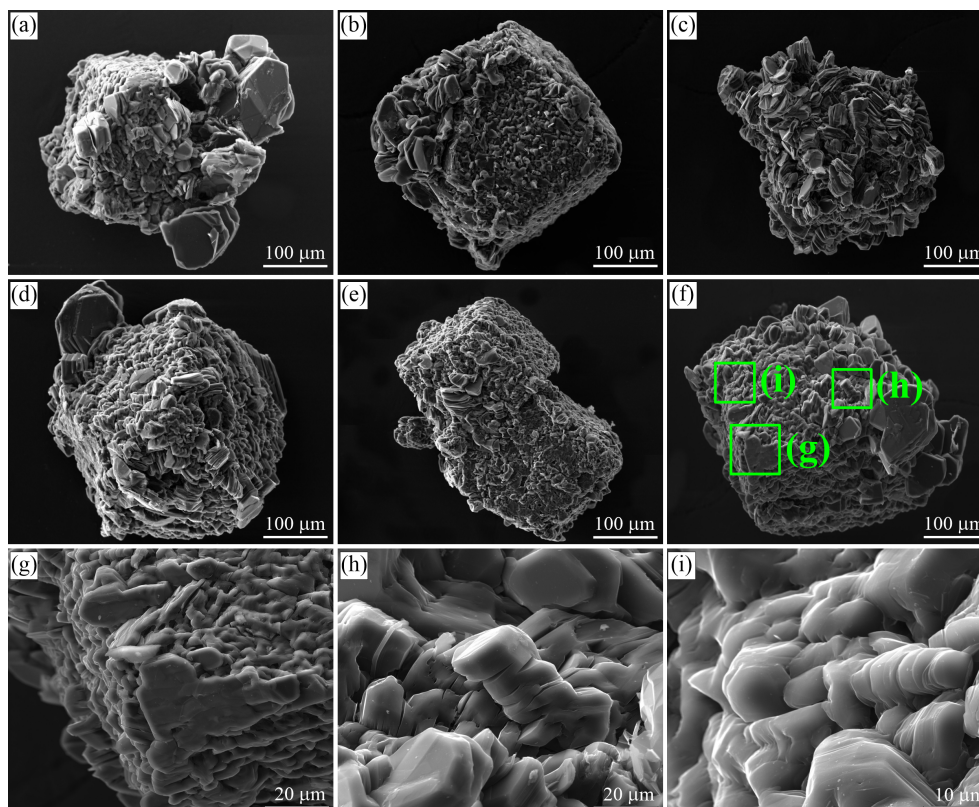


**Figure 3.** SEM SE images of graphite cuboids from the garnet-clinopyroxene rocks of the Kumdy-Kol microdiamond deposit. Graphite crystals with a different “a/c” aspect ratio can be observed on cuboids. Large euhedral graphite crystals tend to concentrate at the cuboid apices (a–g). Prismatic graphite crystals (h,i) usually growing from the supersaturated liquids are quite abundant among flake graphite grains.

Graphite cuboids (Figure 3) consist of coarse-grained graphite aggregates (sub-individuals are up to 50  $\mu\text{m}$  in size). Large euhedral graphite crystals tend to concentrate at the cuboid apices (Figure 3a), while the rest of the {100} surface is composed of relatively uniform graphite crystallites (Figure 3b). Neither graphite cuboids, nor graphite crystallites display any dissolution features on the (0001) surfaces (Figure 3).

The morphologies of diamond and graphite cuboids from the diamond-bearing marbles (Kumdy-Kol deposit) are similar to those from the garnet-clinopyroxene rocks, but the crystal size of diamond and graphite in the marbles is significantly smaller (2–45  $\mu\text{m}$ ) [41,68,84,87].

### 3.1.2. Gneisses and K-Feldspar–Tourmaline–Quartz Rocks

In the garnet–biotite, garnet–clinopyroxene, garnet–kyanite–phengite gneisses from the Kokchetav massif, diamonds occur as cuboids with a varied morphology of the {100} surfaces [68,80,83,88]. Octahedral diamond crystals with sharp edges can be found [22,76,89] only in the clinozoisite gneisses (Figure 4) and some tourmaline-rich K-feldspar–tourmaline–quartz rocks (Figures 5 and 6).



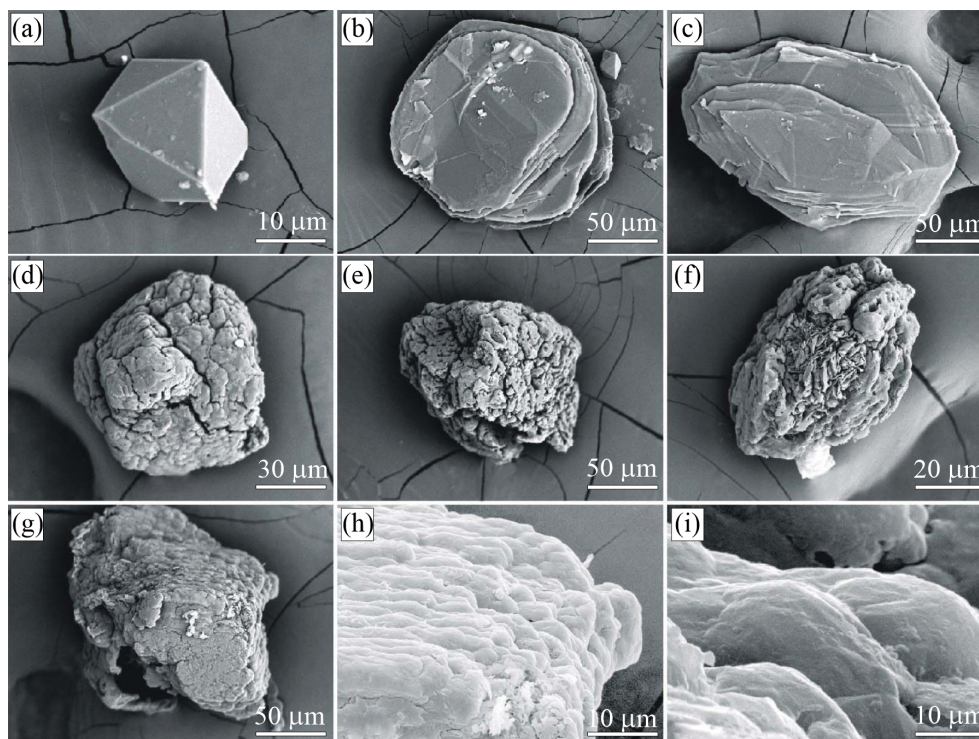


**Figure 4.** SEM SE images of diamond (a) and graphite (b–i) from the clinozoisite gneisses of the Barchi-Kol area. The predominant diamond morphology within this rock type is octahedral, while large graphite cuboids sporadically occur as inclusions in garnet, zircon, and the rock matrix. Hexagonal euhedral graphite flakes, as well as booklets are the predominant graphite morphologies occurring in the matrix and as inclusions in refractory minerals.

In contrast to the garnet–clinopyroxene rocks and marbles, all gneisses have a graphite content much higher than diamond. Generally, graphite occurs as euhedral flakes, having a relatively uniform distribution within the rocks. In some samples, there are bands (Figure 5) and lenses enriched in graphite (see for the details Figure 2 in [37]). Diamond and graphite crystals are concentrated within the same zones. Diamonds from the sample 2018G36 are perfect octahedrons (Figure 5) that occasionally occur as intergrowths with hexagonal graphite flakes. Figure 5b shows the 0001 face of a graphite crystal perpendicular to a {111} diamond face.

Graphite cuboids from the Kumdy-Kol gneisses occur either as individual grains or their intergrowths (Figure 7f). Although the size of the graphite cuboids is comparable with that of the diamond crystals, in most cases, the graphite grains are larger than those of the diamond. SEM images of thermo-chemically-extracted graphite (up to 300 μm) and diamond (up to 50 μm) cuboids from the Kumdy-Kol gneisses are presented in Figures 7 and 8, respectively. Both the diamond {100} surface and the graphite {0001} pinacoid plane have a rather complicated morphology. Diamond surfaces have small hills (Figure 8a,b) and depressions (Figure 8c). The pinacoid plane {0001} of some graphite crystals is covered with smaller randomly-oriented graphite crystals (Figure 7a,b). We have not recognized any features of spiral growth on the pinacoid plane of graphite crystals similar to that reported in [48,90]. Some graphite cuboids are composed of coarse-grained aggregates, while others comprise a suite of smaller cuboids, in which individual graphite flakes can be hardly distinguished by optical and scanning electron microscopy.

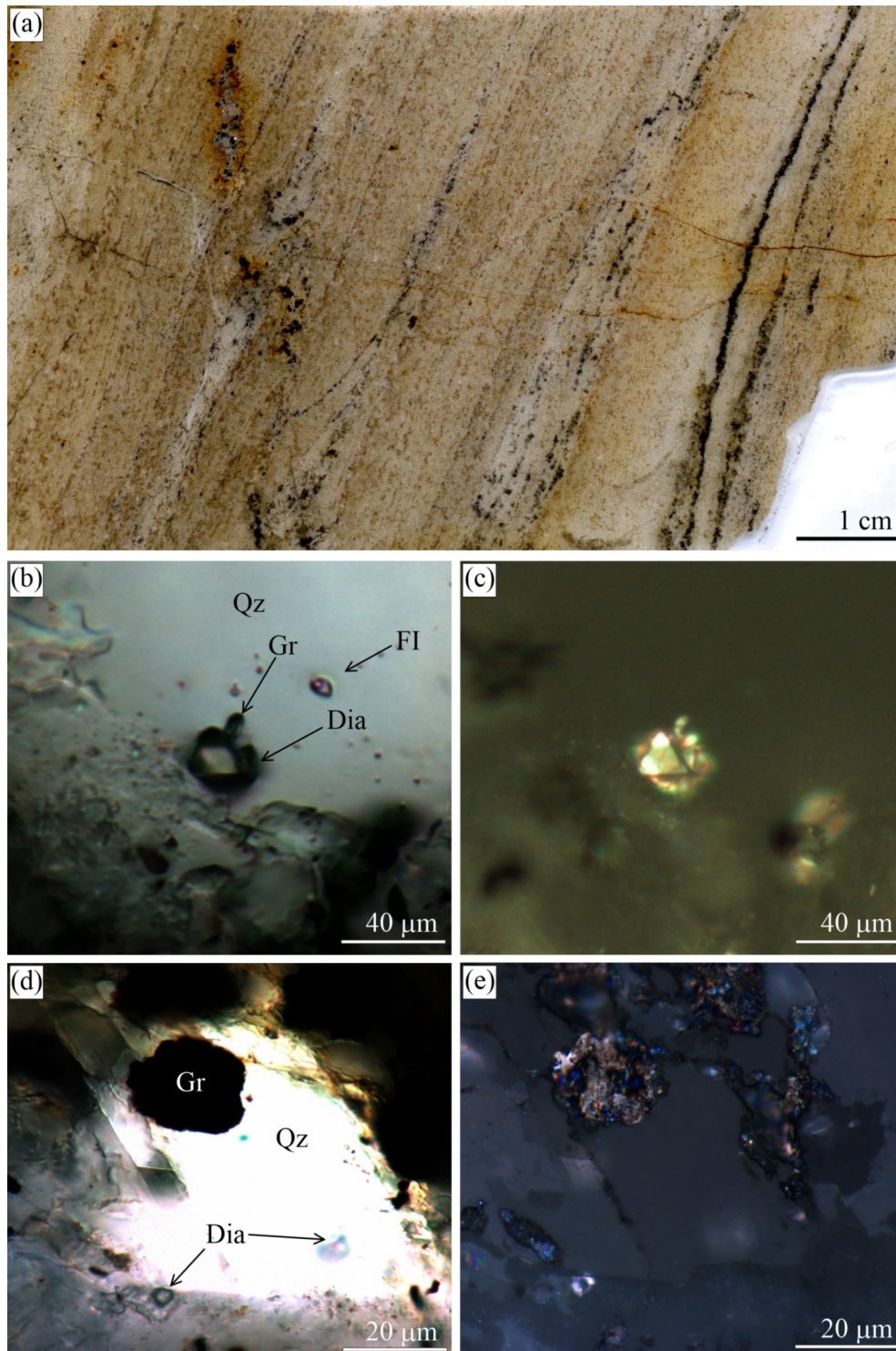


**Figure 5.** (a) Scanned thin section of a K-feldspar-tourmaline-quartz rock (sample 2018G36) with black zones enriched in graphite (Kumdy-Kol microdiamond deposit). Transmitted (b,d) and reflected (c,e) light images of the graphite-diamond relationships in this sample. Images (b,c) and (d,e) depict the same fields, respectively. FI = fluid inclusion.



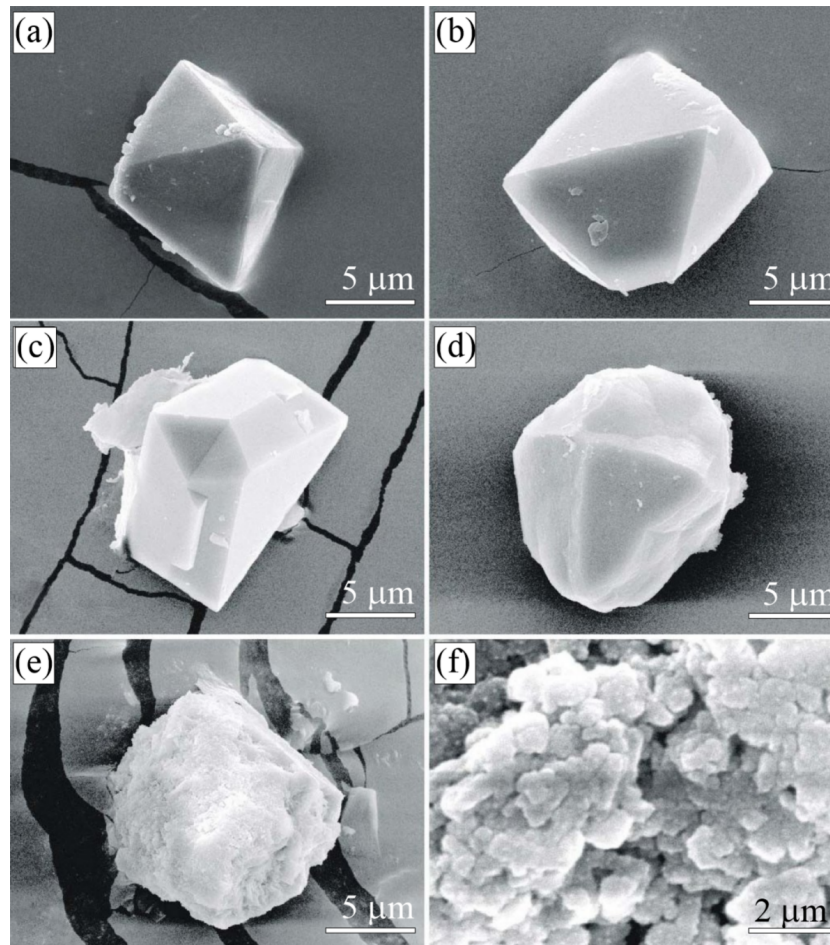


**Figure 6.** SEM SE images of diamond (a–d) and graphite (e,f) in the K-feldspar-tourmaline-quartz rocks (Sample G31) from the Kumdy-Kol microdiamond deposit. Diamond occurs as individual octahedral (a,b), twins (c), or cuboctahedral (d) crystals. Graphite cuboids (e) from this sample consist of smaller cuboids  $< 2 \mu\text{m}$  in size (f).

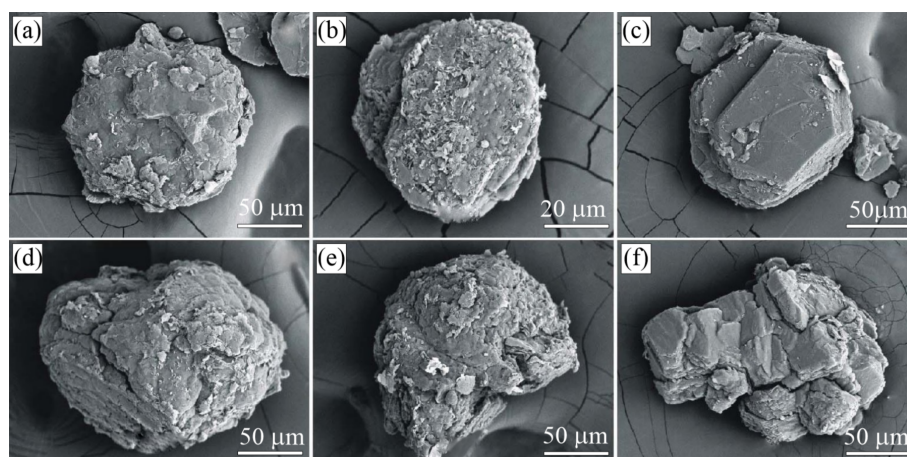


**Figure 7.** SEM SE images of graphite flakes (a–c) and graphite cuboids (d–f) from the sample G11 (Kumdy-Kol microdiamond deposit). Note that the graphite {0001} surface is either curved (a,b) or flat (c). Graphite cuboids exhibit curved (d,e) and flat (f) {100} surfaces, as well.

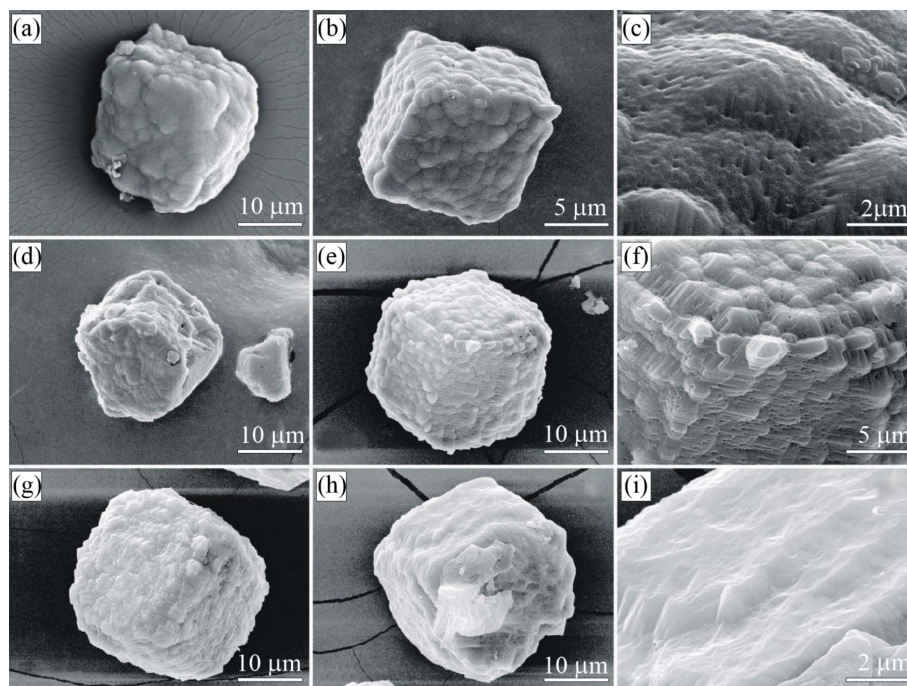


**Figure 8.** SEM SE images of diamond crystals from the sample G11 (Kumdy-Kol microdiamond deposit) [37]. Note that diamond crystals exhibit a diverse morphology of the {100} surface. (a–c) Diamond cuboids with the {100} surface consisting of numerous hillocks, variable in size and shape. (d–f) Diamond cuboids with abundant small {111} facets on cuboid faces. (g–i) Diamond cuboids with a relatively flat {100} surface.

### 3.2. Estes Quarry

The Estes Quarry (West Baldwin, Cumberland County, ME, USA) exposes a granite pegmatite hosting more than forty mineral species, including sulphides (arsenopyrite, chalcopyrite, galena, molybdenite, pyrite, pyrrhotite, sphalerite) and graphite [91]. The samples from the Estes Quarry were provided by G.T. Bearss and represent blocks of albite cross-cut by the graphite veins (Figure 9).

Graphite occurs as spheres and somewhat less commonly as cuboids (Figures 9b–e and 10), but locally, the segregation of graphite cuboids constitutes massive aggregates (Figure 9a). The spherical and cuboid graphite aggregates show smooth surfaces (Figure 10c,d), while their internal radial textures are due to relatively coarse-grained graphite flakes radiating from a common center (Figures 9e and 10b).

### 3.3. Maksyutov Complex

The Maksyutov complex (South Ural, Russia) is a subduction zone metamorphic terrane that formed upon the closure of the Uralian Ocean during the Late Paleozoic [92]. The Maksyutov complex is the first among high-pressure metamorphic complexes, where the presence of coesite was suspected by Chesnokov and Popov [93]. Later, Leech and Ernst [94] described graphite cuboids (up to 1.5 cm in size) from this complex and interpreted them as pseudomorphs after diamond. So far, however, the UHPM origin of the complex has not been confirmed by an independent investigation [62]. For our study, the samples of a “graphitic schist” were picked from the same localities as described in [94], for which the blueschist facies conditions of about 1.5–1.7 GPa and 600 °C have been proposed [62,94]. The protolith of these rocks was likely a black shale subducted to a depth of about 60 km. However, in some samples, the alternation of eclogite-blueschist lithologies and “graphitic schist” can be observed (Figure 11).



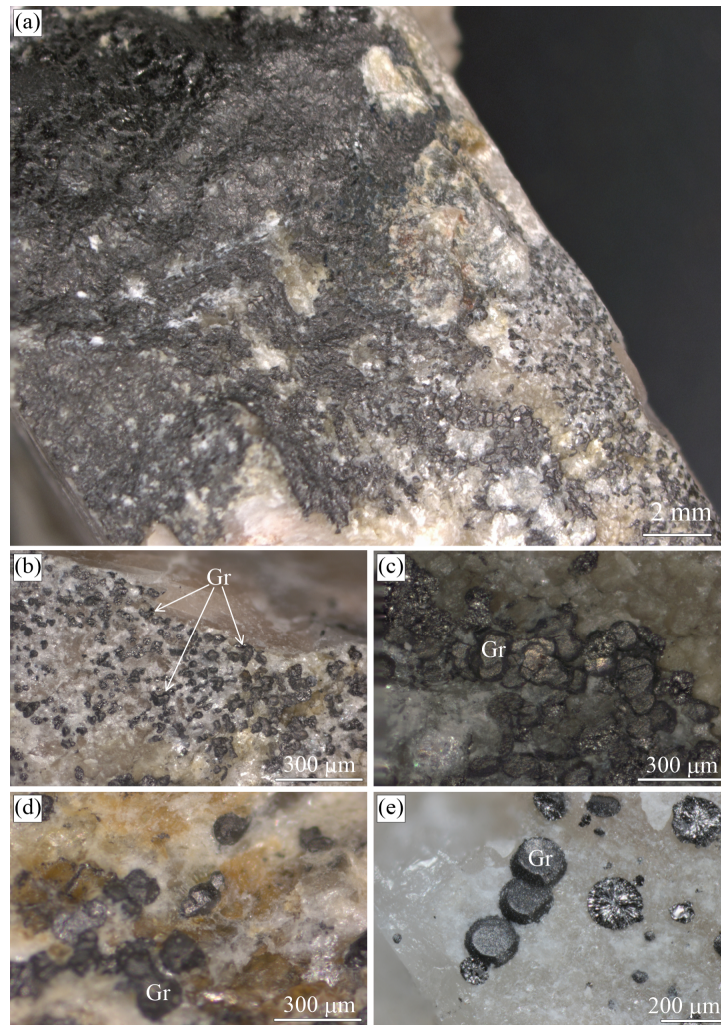


**Figure 9.** Photographs of the graphite-bearing sample from the Estes Quarry, USA. Sample overview (a). Graphite cuboids appear as individual grains or their intergrowths, locally as massive aggregates (b–e).

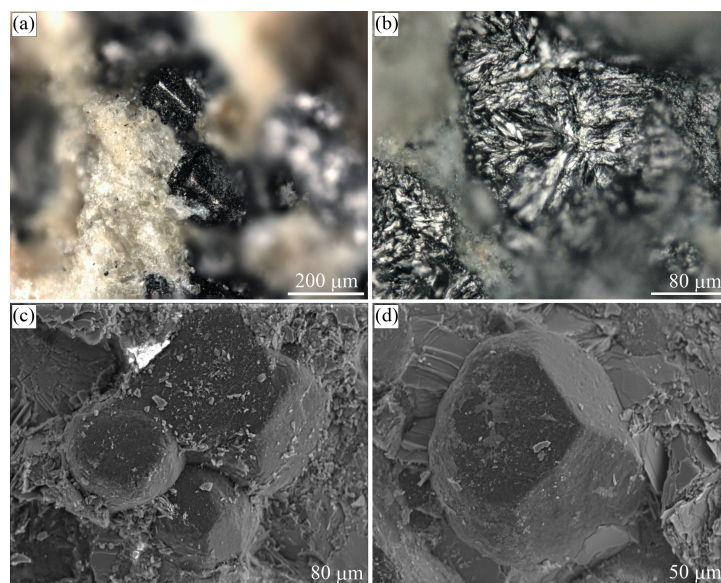


**Figure 10.** Optical (a,b) and SEM SE (c,d) images of the graphite cuboids from the Estes Quarry, USA, illustrating their morphology and radial internal texture.



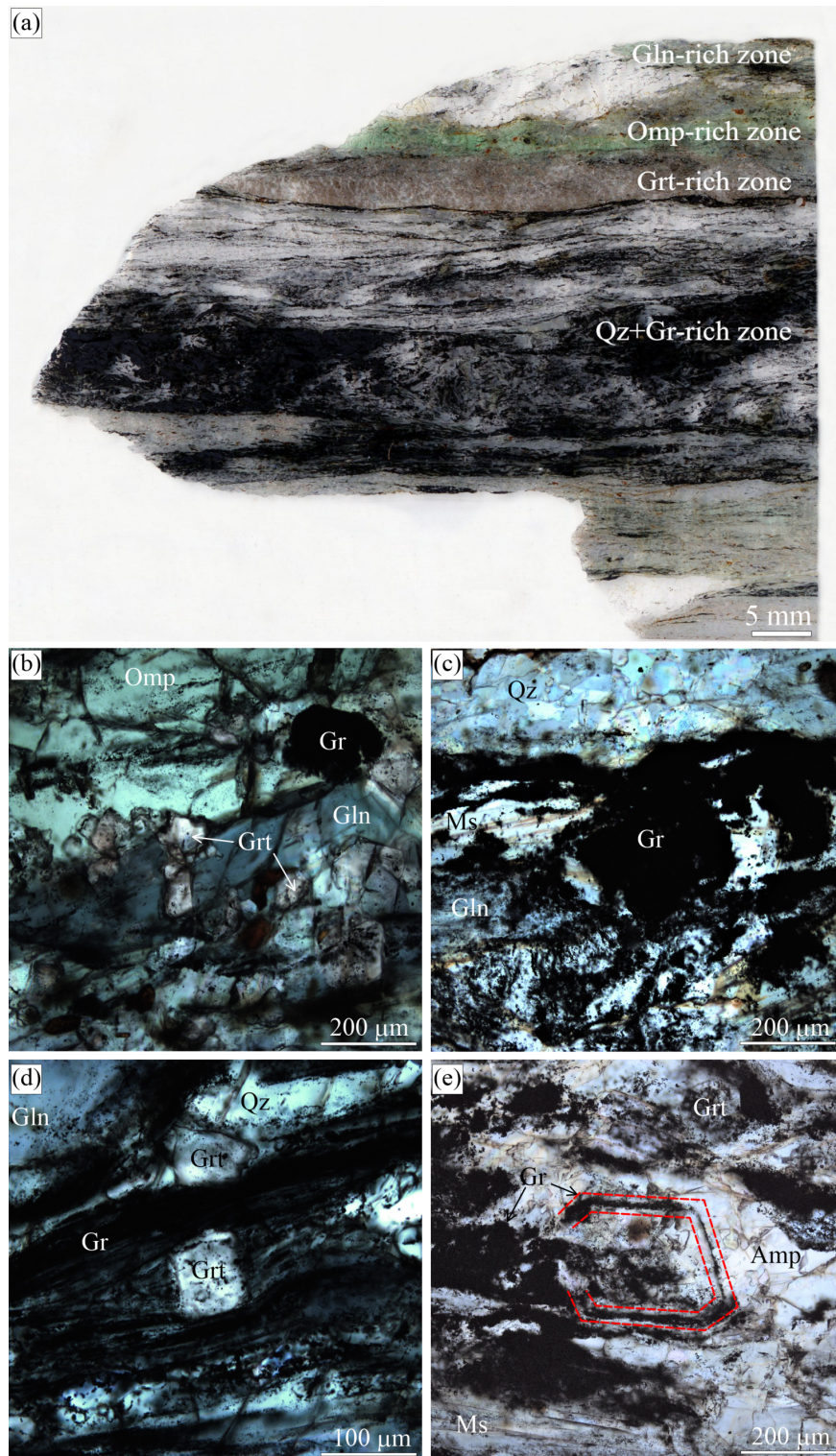


**Figure 11.** (a) Scanned image of the eclogitic sample with alternation of different zones enriched in omphacite, garnet, glaucophane, and graphite from the Maksyutov complex. Transmitted light images showing (b) large graphite cuboid surrounded by omphacite, garnet, and glaucophane and fine-grained graphite inclusions in these minerals, (c) large graphite cuboid in quartz-, and glaucophane-rich layer, (d) the spatial graphite distribution in high-pressure minerals (garnet and glaucophane) and quartz matrix, and (e) atoll-like graphite cuboid (outlined in red) with the mineral assemblages occupying the core of this cuboid and the matrix mineral assemblages being the same.



The “graphitic schist” consists of graphite (up to ~40 vol. %), quartz (~40 vol. %), small euhedral garnet porphyroblasts (~10 vol. %) and phengitic mica (~10 vol. %); pyrite, glaucophane, and rutile occur as accessory minerals (Figure 12).

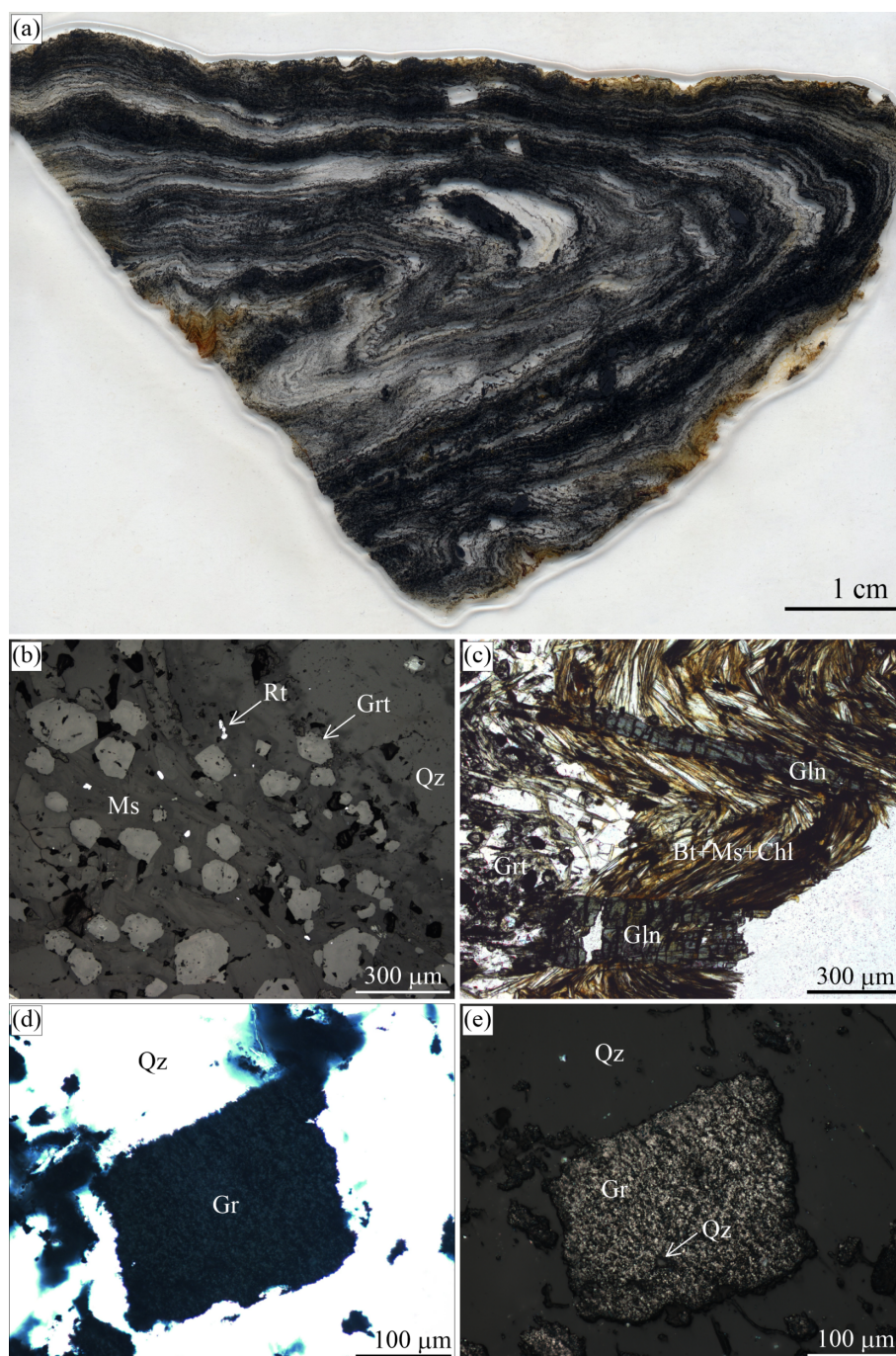


**Figure 12.** (a) Scanned image of the foliated “graphitic schist” from the Maksyutov complex. Reflected (b) and transmitted (c) light images showing characteristic mineral assemblages of the “graphitic schist”. The graphite cuboid enclosing quartz inclusions displayed in transmitted (d) and reflected (e) light.

Graphite forms small euhedral crystals and cuboids up to 15 mm across. Graphite cuboids encompass abundant quartz inclusions (Figure 12e), while anhedral graphite inclusions are enclosed in garnet porphyroblasts. Massive and atoll-like graphite cuboids occur together in the individual samples (Figure 11). The former are made up of small randomly-oriented graphite crystals (up to 3 µm). We have not observed any variations in the grain size of these graphite crystals inside individual

graphite cuboids from the core to rim (Figure 13). Occasionally, graphite crystals are composed of spiral-like intergrowths (Figure 13f), but no traces of spiral crystal-growth mechanism have been detected on the {0001} plane of individual graphite cuboids. There are some graphite cuboids that show radial textures (Figure 13i,j) similar to graphite spherulites. As a rule, the {100} graphite cuboid surfaces resemble the morphology of diamond cuboids (see, for example, Figure 8 in [22]). Atoll-like graphite cuboids consist of graphite-rich aggregates of matrix minerals outlined by almost pure fine-grained graphite aggregates, the latter being surrounded by graphite-depleted matrix (Figure 11e).

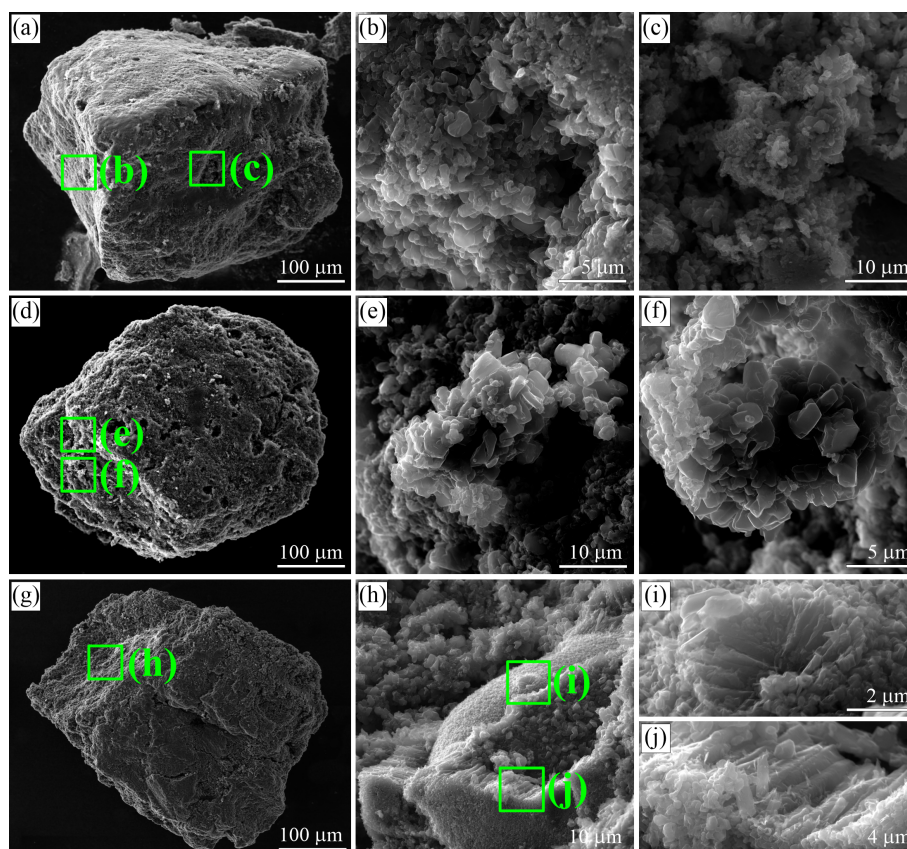


**Figure 13.** SEM SE images depicting the morphology (a–g) and internal structure (h–j) of graphite cuboids from the “graphitic schist” (Maksyutov complex). Note the “macrospiral-like” graphite aggregate (f) and radial polycrystalline textures (i,j).

### 3.4. Beni Bousera Complex

The graphite-bearing samples from the Beni Bousera complex (Morocco, Northern Africa) were collected during the pre-conference excursion of the Lherzolite conference in 2014 organized by Prof. Carlos J. Garrido (IACT, Granada, Spain). Unfortunately, we were not completely sure if the samples studied by Slodkevich [35,36] and Pearson et al. [95] came from exactly the same localities. The Beni Bousera pyroxenites consist of orthopyroxene (~60 vol. %) and garnet (~40 vol. %), and the accessory minerals are graphite and sulphides. The detailed petrographic description of these rocks was given by El Atrassi et al. (see [63] and the references therein), who reported microdiamonds in samples from this locality. In our samples, graphite occurs as euhedral flakes and occasionally as massive aggregates (Figure 14), but neither microdiamonds, nor the graphite aggregates of octahedral/cuboid morphology similar to those described in [35,36,95,96] have been recognized yet. Our efforts at using thermo-chemical dissolution of small rock blocks has proven unsuccessful in obtaining a graphite crystal with the cuboid or octahedral morphology, as well (Figure 14). There appears to be no preferred orientation of graphite crystals within the studied graphite aggregates (Figure 14d).



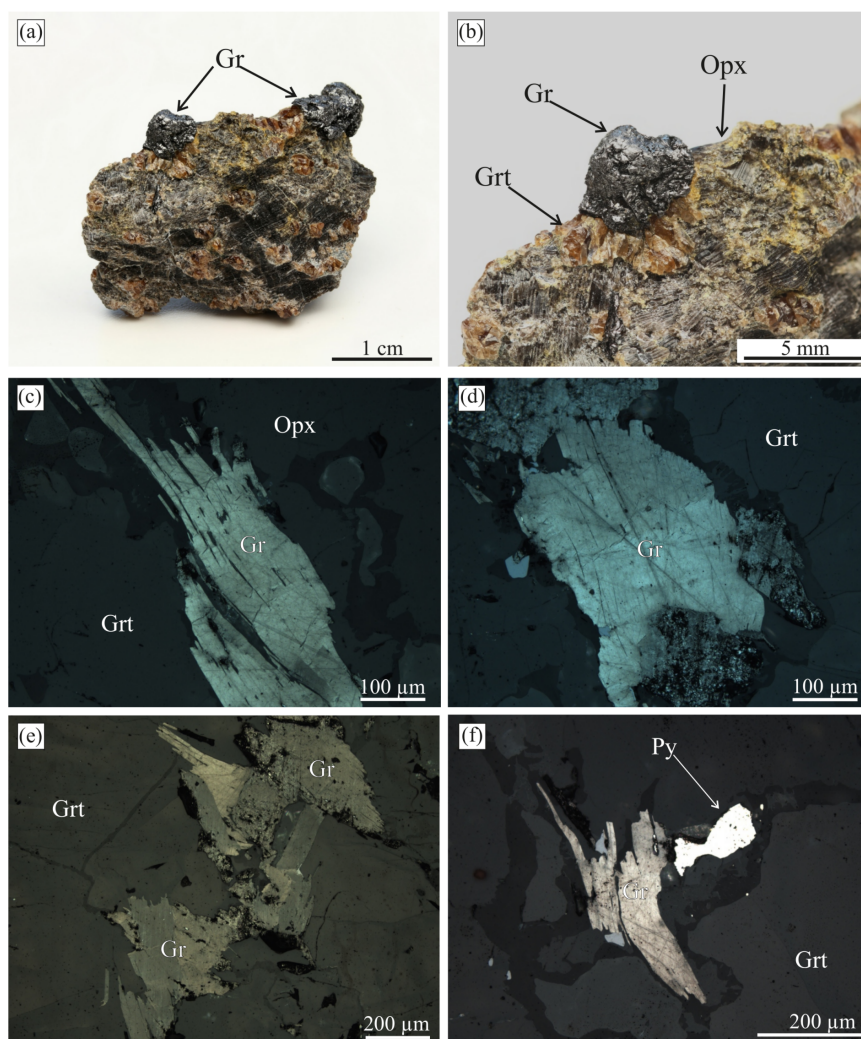


**Figure 14.** (a,b) Photographs of a graphite-bearing sample from the Beni Bousera complex. Graphite aggregates are exposed at the surface by thermo-chemical extraction. (c–f) Reflected light images showing the internal graphite texture in the same sample.

The  $\delta^{13}\text{C}$  isotopic composition of the graphite aggregates is rather homogeneous and ranges from  $-24.9$  to  $-25.1\text{‰}$ . These results are in a good agreement with the isotopic data for the graphite pseudomorphs after diamond (from  $-16$  to  $-27.6\text{‰}$ ) in the Beni Bousera rocks reported by Pearson et al. [97].

### 3.5. Oznernaya Mountain Intrusion

The Dzhaltul igneous complex (Russia) is unique among the trap intrusions of the Siberian Platform and represents a tholeiite-basalt melt that differentiated from picritic gabbro–dolerite to quartz monzonite. The complex is known for its native iron, magnetite, and sulphide mineralization [25]. The Oznernaya mountain intrusion belongs to the Dzhaltul complex and hosts graphite-bearing rocks containing native iron (Figure 15). Details on the petrology and geochemistry of these mineral assemblages have been published elsewhere (see [25] and the references therein).

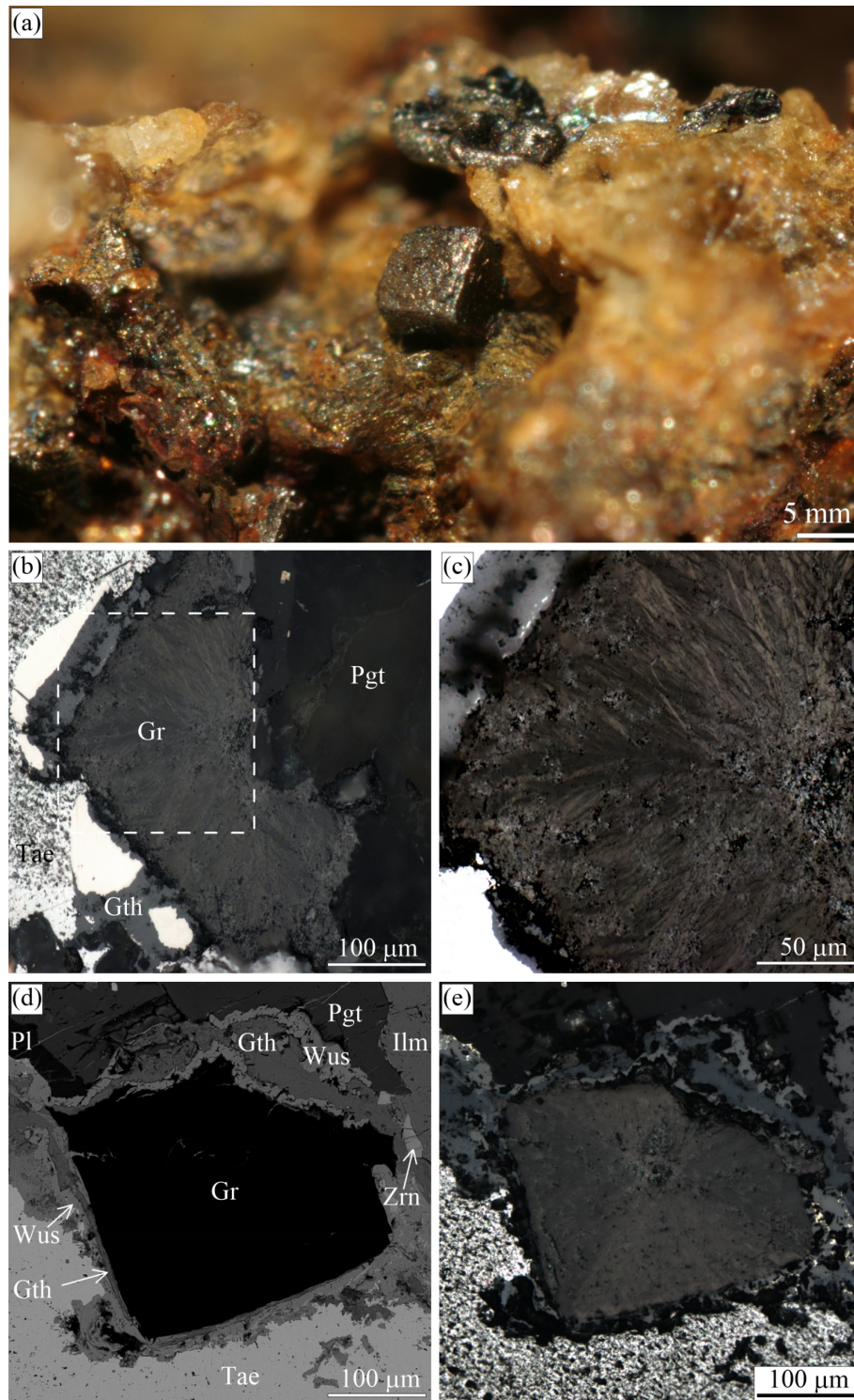


**Figure 15.** Images of graphite-bearing samples from the Ozeraya mountain intrusion (Norilsk, Russia). (a) Optical image of the graphite cuboid exposed by the acid dissolution of native iron. (b,c,e) Reflected light images of the internal morphology of graphite cuboids. Figure (c) depicts the outlined area of (b). (d) SEM BSE image of graphite cuboid shown in (e). Note that in (c,e), the polars are parallel, so the orientation of the bright sectors are aligned with the graphite/graphene layers parallel to the direction of the electric field polarization.

Graphite cuboids (cliftonite) from this locality were first reported in [98,99]. These graphite cuboids (up to 500 μm in size) appear as individual crystals of cubic habit or cube intergrowths.



They typically occur in “droplets” of native iron, extending from the surrounding silicate minerals towards metallic “droplets” (Figure 15b). In our samples, the mineral assemblages coexisting with graphite cuboids consist of cohenite, kamacite, wustite, taenite, ilmenite, plagioclase, and pigeonite (Figure 15). SEM study of the graphite external morphology revealed this type of graphite cuboids (cliftonite) to have a well-defined flat or blocky/mosaic {100} surfaces (Figure 16).

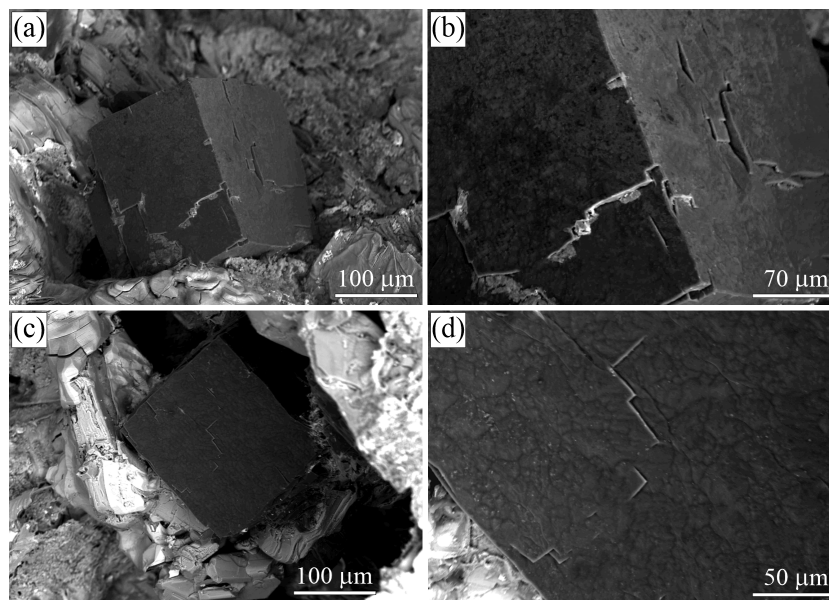


**Figure 16.** SEM SE images of the graphite cuboids from the Ozernaya mountain intrusion (Norilsk, Russia). (b,d) are magnified fields of (a,c), respectively.

#### 4. Raman Spectroscopy

The Raman spectrum of graphite contains first-order ( $1100\text{--}1800\text{ cm}^{-1}$ ) and second-order ( $2500\text{--}3100\text{ cm}^{-1}$ ) regions [100–105]. The main Raman band in the graphite spectrum is the  $E_{2G2}$  vibration mode G ( $1580\text{ cm}^{-1}$ ). In the poorly-ordered carbonaceous material or disordered graphite, the additional D1 ( $1350\text{ cm}^{-1}$ ) and D2 ( $1620\text{ cm}^{-1}$ ) Raman bands or so-called defect bands testify to the in-plane defects and heteroatoms ( $O_2$ ,  $N_2$ , H) in the graphite structure [23,29]. The main peaks of a second-order region in the graphite Raman spectrum are  $2400$ ,  $2700$ ,  $2900$ , and  $3000\text{ cm}^{-1}$ , which result from the overtone and combination scattering [101,104]. Beyssac et al. [105] proposed the use of the R1 and R2 ratios as a means of estimating the degree of graphite crystallinity, where R1 is a peak height ratio and R2 is a peak area ratio. Raman spectroscopic methods have been employed to study the thermo-chemically-extracted graphite cuboids, as well as unexposed inclusions and the polished graphite cuboids in thin sections. The spectral results are presented in Figures 17–20 and summarized in Table 2.

We observed some variation in the Raman spectra of samples prepared using different techniques (i.e., thermo-chemical extraction and polishing). The largest differences in the defect-band intensities between thermo-chemically-extracted graphite and polished ones have been detected in the diamond-bearing garnet-clinopyroxene samples from the Kokchetav massif (Figure 17). For the thermo-chemically-extracted graphite cuboids from the Kokchetav garnet-clinopyroxene rocks, there is a good correlation of the full width at half maximum (FWHM) and the position of the D1 and G peaks from center to the rim of graphite cuboids (Figure 17b). The variations in graphite crystallinity degree within the individual graphite cuboid are rather small. The Raman spectrum of the thermo-chemically-extracted graphite grains is characterized by a low intensity of the D1 band, while the intensity of this band in polished graphite is significantly higher, being comparable with that of the G-band (Figure 17b,d). FWHM values ( $FWHM_G = 16\text{ cm}^{-1}$ ) of thermo-chemically-extracted graphite crystals are roughly two-times lower than those of polished samples ( $FWHM_G = 34\text{ cm}^{-1}$ )

(Figure 17b,d). This evidence clearly indicates the effect of polishing during the sample preparation on the graphite Raman spectrum, which causes the increase of the defect band intensity.

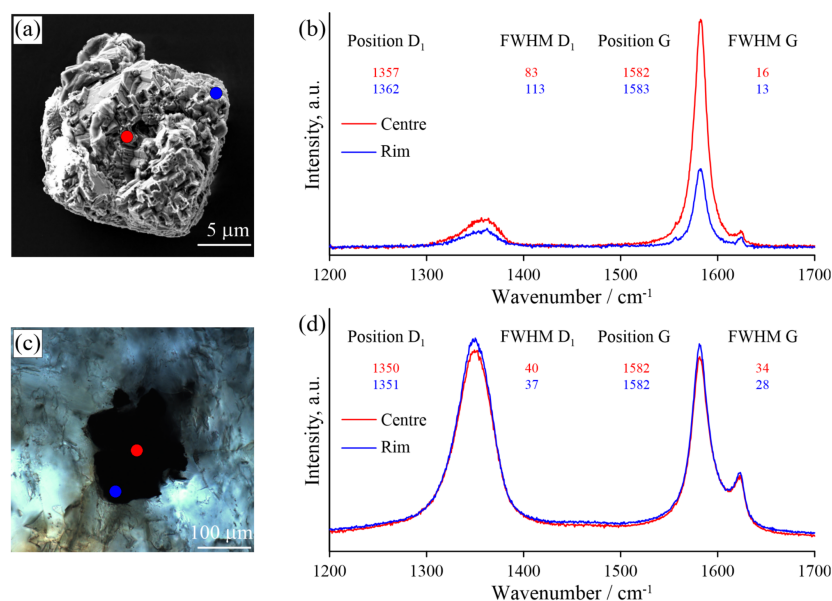


**Figure 17.** Optical images (a,c) and Raman spectra (b,d) obtained for thermo-chemically extracted (a) and polished (c) graphite cuboids from the Kumdy-Kol garnet-clinopyroxene rocks (Kokchetav massif).

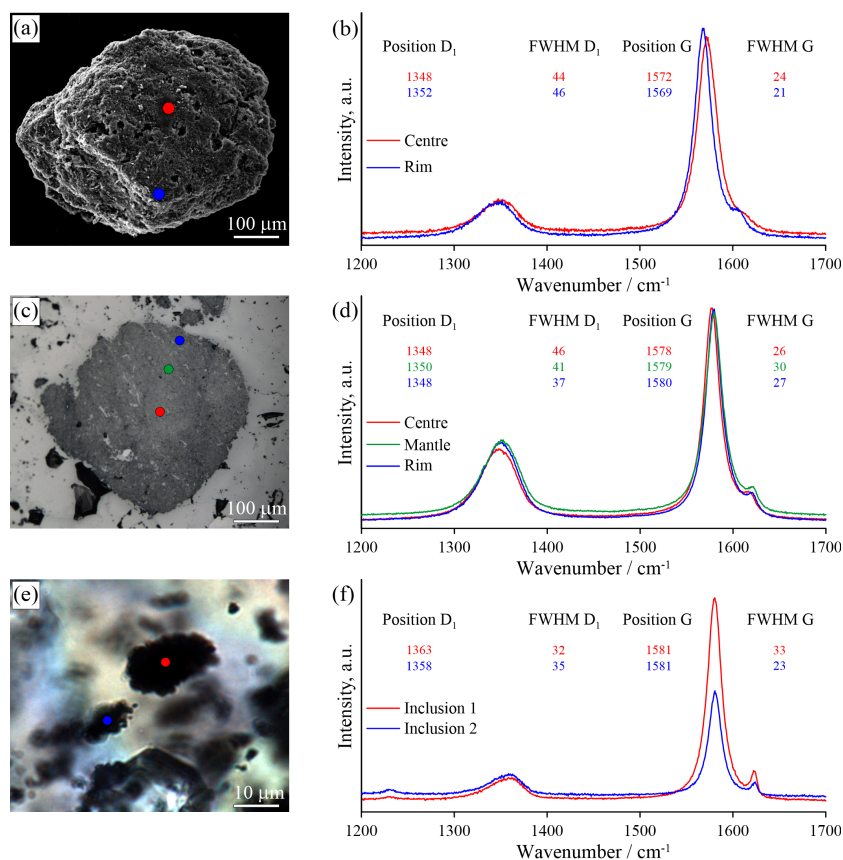


**Figure 18.** Optical images (a,c,e) and Raman spectra (b,d,f) recorded for thermo-chemically-extracted (a), polished (c), and unexposed (e) graphite cuboids from the Maksyutov complex.



For the thermo-chemically-extracted graphite cuboids from the Maksyutov complex, there is an increase of the  $\text{FWHM}_{D1}$  and an upshifting of the D1 peak with a simultaneous decrease of the  $\text{FWHM}_G$  and a downshifting of the G peak from core to rim (Figure 18b). For the polished graphite cuboids, there are no regularities in the variations of the D1 and G peak positions and the FWHM. For unexposed graphite inclusions, there are significant variations in the FWHM values of the D1 and G peaks, even for inclusions occurring within a distance of several microns (Figure 18e,f). The differences in Raman spectra of graphite from the Maksyutov complex prepared by different techniques are less significant compared to those in the Kokchetav samples.

The two Raman traverses from the core to rim of polished graphite cuboids from the Ozernaya samples do not reveal any clear regularities in variations of the graphite Raman spectra (Figure 19). Only in some instances is an upshifting of the D1 and G peaks observed. Raman spectroscopic study of intact graphite cuboids (Figure 19e,f) demonstrates similar results with the data obtained from polished samples. The D1 and G peak positions and their FWHM are almost the same, although the peak intensity ratios are different (Figure 19e,f). The study of unexposed graphite cuboids from the Ozernaya samples was hindered because of the opaqueness of the host minerals (Figures 15 and 19).

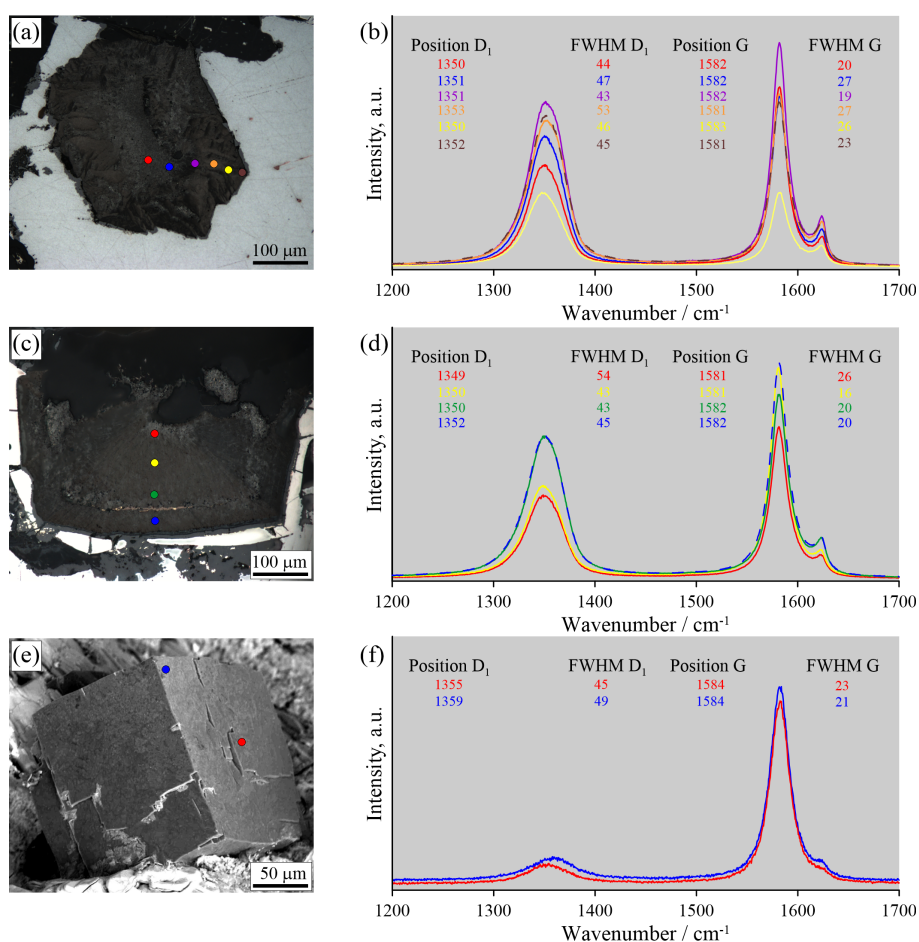


**Figure 19.** Optical images (a,c,e) and Raman spectra (b,d,f) obtained for polished (a–d) and intact (e,f) graphite cuboids from the native iron-bearing Ozernaya samples. The color of Raman spectrum corresponds to the color of the spot where Raman spectrum was acquired.

Raman study of the intact graphite cuboids and the cores of the broken graphite cuboids from the Estes Quarry revealed the external part of graphite cuboids to be more defective (Figure 20). The external part of the graphite cuboids exhibits a Raman spectrum characterized by a large G band around  $1580\text{ cm}^{-1}$ , usually encompassing both the G band and the D2 band. The D1 band is also

quite broad ( $>36\text{ cm}^{-1}$  FWHM) and more intense compared to that of the intact graphite cuboids from other localities.

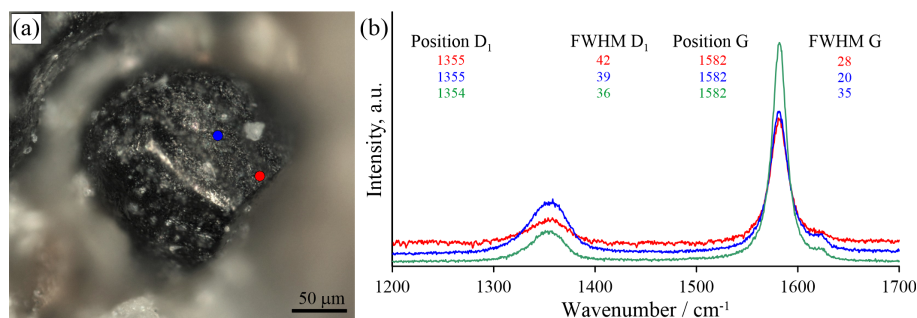


**Figure 20.** Optical image (a) and Raman spectra (b) obtained for the intact graphite cuboids from the Estes Quarry. Blue and red spectra were collected at the {100} surface of the intact graphite cuboid (a), and a green spectrum was recorded in the core zone of the broken graphite cuboid (see Figure 10b).

The Raman-based graphite geothermometer ([105], hereafter referred to as  $T_{Gr}$ ) was used to estimate the formation temperatures of intact graphite cuboids from the samples studied (Table 2). The lowest temperature estimates ( $470\text{ }^{\circ}\text{C}$ ) were obtained for graphite cuboids in the pegmatitic samples from the Estes Quarry. The Kokchetav samples yielded similar values ( $470\text{ }^{\circ}\text{C}$ ), consistent with the previous results [80]. Temperature estimates for intact graphite cuboids from the “graphitic schists” of the Maksyutov complex are as high as  $550\text{ }^{\circ}\text{C}$ . The highest temperature assessments ( $625\text{ }^{\circ}\text{C}$ ) were deduced for graphite cuboids from the Ozernaya magmatic rocks.

**Table 2.** Average parameters obtained from the Raman spectra of thermo-chemically-extracted graphite cuboids from different localities.  $R1 = D1/G$  peak intensity (i.e., peak height) ratio,  $R2 = D1/(D1 + D2 + G)$  peak area ratio,  $T_{Gr}(^{\circ}\text{C}) = -445 \times R2 + 641$  [105].

Sample Locality	Peak Position D1	Peak Position G	FWHM D1	FWHM G	R1	R2	$T_{Gr}(^{\circ}\text{C}, \pm 50^{\circ}\text{C})$
Estes Quarry	1355	1582	39	20	0.36	0.38	470
Kokchetav massif	1357	1582	83	16	0.16	0.38	470
Maksyutov complex	1360	1580	43	28	0.15	0.2	550
Ozernaya	1355	1584	45	23	0.06	0.03	625

## 5. Discussion

### 5.1. Temperature Constraints on the Graphite Cuboid Crystallization

The temperature values obtained by  $T_{Gr}$  vary not only between the studied complexes, but also within the individual samples [80]. It should be noted that only for graphite cuboids from the Maksyutov complex are the temperature estimates determined by  $T_{Gr}$ , in a good agreement with the previous temperature values yielded by the garnet-clinopyroxene geothermometer for the peak metamorphic conditions [62,94]. The lowest temperature estimates ( $470\text{ }^{\circ}\text{C}$ ) were obtained for graphite cuboids in the pegmatitic samples from the Estes Quarry, consistent with the graphite formation along cracks in the albite from impregnating fluids well past the albite formation. The application of  $T_{Gr}$  to the studied Kokchetav samples gave temperature values  $\sim 470\text{ }^{\circ}\text{C} \pm 50\text{ }^{\circ}\text{C}$ , which are significantly lower than the temperatures obtained by the garnet-clinopyroxene [55,56,58,71,74], Ti-in-zircon, and Zr-in-rutile [61,80] geothermometers for the peak metamorphic conditions ( $1000\text{--}1100\text{ }^{\circ}\text{C}$  and  $P = 5\text{--}7\text{ GPa}$ ). Occasionally, some graphite cuboids in the Kokchetav rocks occur as intact inclusions associated with pure diamond in K-bearing clinopyroxene with  $\text{K}_2\text{O}$  contents of about 1.5 wt % [22], indicating their formation in the temperature range of  $1200\text{--}1500\text{ }^{\circ}\text{C}$  and pressure of  $>>4\text{ GPa}$  [106].

The temperatures estimated previously for the cliftonite crystallization in the Ozernaya rocks are as high as  $950\text{--}1200\text{ }^{\circ}\text{C}$  (see [25] and the references therein). These temperature assessments are



about 300–600 °C higher than the values obtained by  $T_{Gr}$  in this study. The discrepancy between the temperature values yielded by  $T_{Gr}$  and those afforded by different geothermometers for the peak metamorphic conditions may indicate that  $T_{Gr}$  cannot be applied to diamond-grade metamorphic rocks, although it shows a very good potential for the rocks that underwent low-T (<650 °C) high or ultrahigh-pressure metamorphism. Nevertheless, the occurrence of graphite cuboids in a variety of geological settings indicates that their crystallization is possible at a wide range of PT parameters and is not restricted to UHPM conditions.

## 5.2. The Effect of S and O on the Graphite Morphology

The modification of flake graphite in gray cast iron to the spherulitic or nodular form in ductile cast iron is of considerable technological importance [107]. The study by Johnson and Smartt [107] revealed that the sulfur and oxygen always present in commercial alloys adsorb at the graphite/melt interface, effectively “stabilizing” the active sites on the graphite basal planes and preventing the spherulitic growth. Contrary to the observation [107], silicates, oxides, and sulphides are quite abundant in all our samples, indicating that the presence of oxygen, sulfur, or sulphides in natural systems does not prevent the spherulitic growth of graphite. The production of cast iron containing spherical graphite, as opposed to flake graphite, usually requires the presence of “nodularizers” such as Ce or Ce and Mg, which seem to promote the nucleation and growth of nodular (spherical) graphite (see [108] and the references therein). Double and Hellawell [109–111] noted that very thin graphite sheets should be able to roll up easily into loose spheres while floating freely in solution due to their extreme flexibility. Further, they proposed that the radial texture and the circumferential alignment of the graphene sheets result from a cone-helix growth mechanism from a common center. Sadocha and Gruzlesky [112] suggested that graphite spheroids in high-purity Fe–C–Si alloys result from the bending of the graphite platelets, through “circumferential growth” or “curved crystal growth” by the movement of steps around the surface of the spheroid. Later Stefanescu et al. (see [113] and the references therein) pointed out that spheroidal graphite can crystallize in high purity Ni–C and Fe–C–Si melts, as well as in “impure” industrial melts, where the level of surface-active anti-compacting elements (O and S) is drastically reduced through additions of reactive compacting elements (e.g., Mg, Ce, Ca). To achieve spheroidization in high purity melts, much higher solidification rates are required as compared to the industrial melts. With increasing purity and solidification rate, a transition from plate-like to spheroidal graphite occurs [113]. The SEM study of graphite cuboids has not revealed any traces of other elements besides carbon in our samples, implying a high crystallization rate.

It has been shown that graphite tends to grow as curved-circumferential plates around the spherical (MgCa)S nucleus [113]. Consequently, a sulphide (e.g., pyrite) or a diamond grain can also potentially serve as a spherical nucleus for further growth of spherical graphite. Based on the similarities of the carbon “onions” observed by Ugarte [114] and the spherical graphite observed in cast iron, where it also has its graphene sheets aligned circumferentially, Miao et al. [115] supposed that the nucleus of spherical graphite in cast iron might be a  $C_{60}$  polyhedron. The occurrence of this unusual carbon form in geological materials seems to reflect very specific conditions of formation summarized by Jehlička et al. [116], including plasma formation during rock transformation due to lightning [117], impact events [118], or specific high-temperature transformation of biogenic carbonaceous matter [119]. Recently, Cruz [120,121] suggested that nanospheres, polyhedral particles, and nanotubes could be the precursor of diamond and tabular- or rod-shaped graphite inclusions in garnets from diamond-grade rocks of the Betic Cordillera, Spain. Unfortunately, the finding of microdiamonds from the Betic Cordillera was not confirmed by an independent study [122]. Hence, the role of fullerenes in the formation of microdiamond and graphite cuboids remains unspecified.

The formation mechanism of graphite cuboids is well constrained only for cliftonite-bearing samples from the Ozernaya mountain intrusion [25,47,123–125]. The study of meteoritic samples indicates that cliftonite originates by precipitation within kamacite [47]. Brett and Higgins [47] have also demonstrated that graphite with a cubic morphology may be synthesized in a Fe–Ni–C alloy

annealed in a vacuum. There is a lack of information about the successful synthesis of cliftonite in oxidized environments.

### 5.3. The Role of COH Fluid in the Graphite Crystallization

COH fluids and melts have been considered as a crystallization media for both graphite and diamond in metamorphic rocks [22,37,40,41,48,57,65,66,68,71,79,126–128]. Moderately oxidizing conditions are favorable for diamond crystallization from COH fluids [51], while in reducing fluids, only graphite precipitates, even under conditions of the diamond stability field [129]. Based on theoretical constraints, Manuella [130] and Manuella et al. [131] argued that nanodiamond and other carbon compounds can originate hydrothermally from COH fluids in serpentinite-hosted hydrothermal systems. The crucial role in the nanodiamond stability was attributed to a crystal size as a function of temperature (see Figure 2 in [130]). It should be noted, however, that graphite cuboids in our study are significantly larger (up to a few millimeters in size) than nanodiamonds; hence, the effect of grain size on the graphite/diamond transition is negligible.

An extensive TEM study of inclusions in UHPM diamonds revealed submicron inclusions of COH fluid, K-Ca carbonates, and apatite [132–135], but no rock-forming minerals have been identified among those phases. The lack of graphite precipitates on the wall of these fluid inclusions implies a very low content of dissolved carbon in the COH fluid. Palyanov et al [136] and Korsakov et al. [48] showed that carbon solubility in COH fluid is very low, even at temperatures as high as 1500 °C. Consequently, the graphite cuboids could not have been precipitated from the primary homogeneous COH fluids captured by garnet or clinopyroxene. The formation of graphite cuboids as a result of diamond recrystallization via dissolution-precipitation processes is also unlikely since there are no differences in the morphology of pure diamond and graphite-coated diamond crystals. Up to now, there are relatively few findings of spiral growth on the (0001) graphite crystal planes (such as those reported in [90,137]), especially in the UHPM environments [22]. The rarity of such findings in these environments may indicate that graphite crystallized from highly supersaturated COH fluid or melt.

### 5.4. The Origin of Graphite Cuboids: Is It Caused by the Diamond Graphitization?

The origin of graphite cuboids in UHPM rocks remains debatable. The generally accepted model for the origin of graphite cuboids in UHPM rocks is the partial graphitization of diamond during the retrograde metamorphic stage [39–41,43–45,138]. So far, the formation of graphite aggregates as products of the diamond graphitization processes is evident only for the Beni Bousera [35,36,96] and Ronda [139] complexes. Indeed, Slodkevich [35,36] reported the graphite aggregates with almost perfect octahedral morphology and even their twins (see Figure 1 in [36]). Similar graphite aggregates have not been reported from other complexes. Unfortunately, there are no published images illustrating the internal morphology of these aggregates. However, sketches presented in Figure 2 in [36] are in a good agreement with the experimental results of diamond graphitization [48,123,140,141]. Graphite aggregates with an octahedral morphology have not been recognized in our samples, even where diamond has a perfect octahedral shape, whereas large graphite cuboids are common in the same samples. One could argue that large diamond crystals grew faster and therefore were more defective and easily transformed to graphite cuboids. On the other hand, the garnet-clinopyroxene samples from the Kokchetav massif have very broad variations of the diamond crystal size, as well as the size of graphite cuboids. Furthermore, there are no regularities in the spatial distribution of graphite cuboids, diamonds with graphite coatings, and pure diamond crystals in samples from the Kokchetav massif (Figure 2). The largest diamond crystals (up to 700 µm in size) do not show any traces of graphite, whereas the smaller diamond crystals may be surrounded by graphite coatings of variable thickness. These coatings consist of graphite aggregates with increasing crystal size from the diamond-graphite interface towards the edges (see Figures 7 and 9 in [22]). Pure diamond crystals and graphite cuboids frequently coexist within the same host mineral (garnet, clinopyroxene) at the micron scale. Contrary to diamond crystals, the graphite cuboids studied here occur in intergrowths with rock-forming minerals



(Figures 2 and 21), including K-bearing clinopyroxene with 1.5 wt %  $K_2O$ , indicating their simultaneous UHPM crystallization [58]. All the observations on the diamond-graphite relationships outlined above allow us to argue against the mechanism of graphite cuboid formation in the studied rocks by the partial diamond graphitization. It is assumed that the graphite cuboid formation proceeded similarly to that of diamond cuboids [142] and was controlled by a fast crystallization rate and a high degree of carbon saturation in the fluid or melt.

We emphasize finally that quartz inclusions are very abundant in graphite cuboids from the Maksyutov complex (Figure 21a,b), as opposed to  $SiO_2$  (coesite) inclusions in diamond that occur only sporadically the world over [143–145]. This evidence indicates that these graphite cuboids crystallized within the quartz stability field and thus are not related to the complete graphitization of former diamond crystals, as has been proposed previously [94].

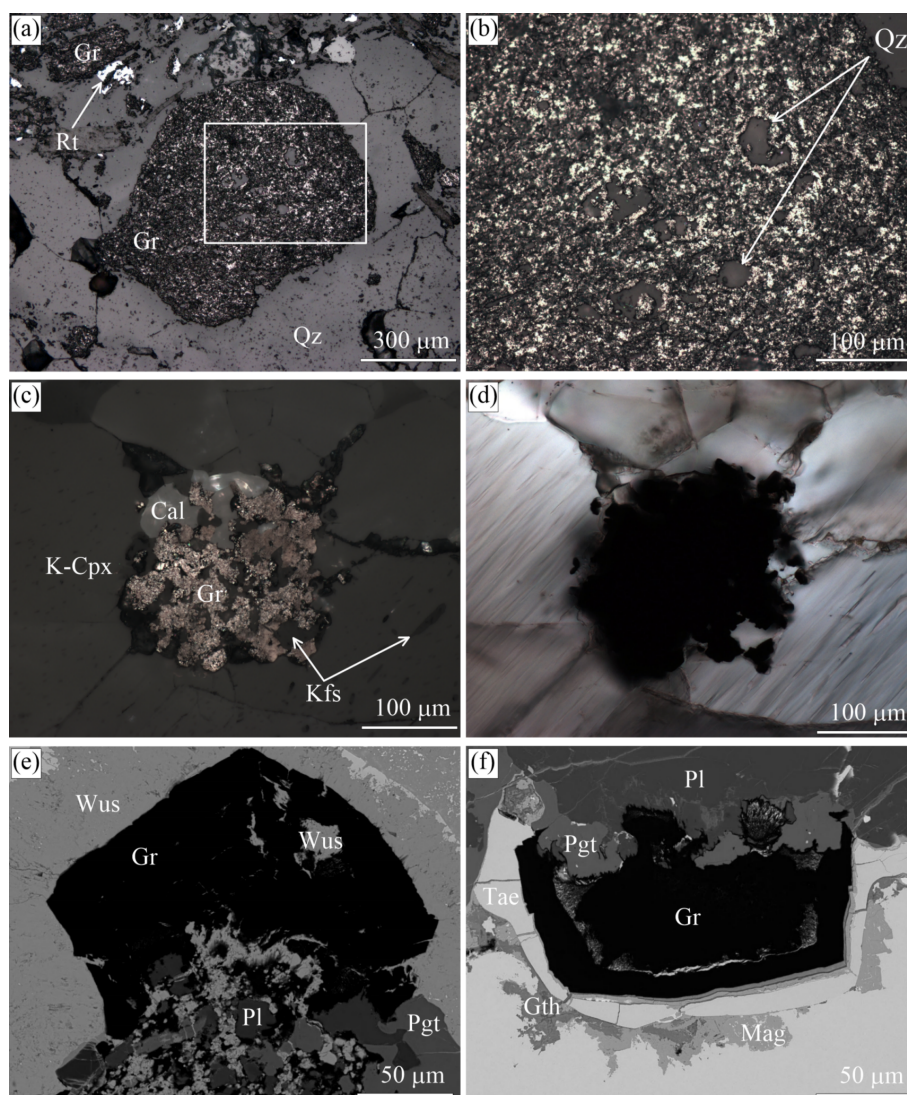


**Figure 21.** Reflected (a–c) and transmitted (d) light images and SEM BSE (e,f) images of the inclusions in graphite cuboids from the Maksyutov complex (a,b), Kokchetav massif (c,d), and the Ozernaya mountain intrusion (e,f). (b) depicts the magnified field outlined in (a). (c,d) depict the same field.

## 6. Concluding Remarks

Graphite cuboids have been identified in natural magmatic and metamorphic samples from different tectonic settings. All studied cuboids represent polycrystalline aggregates composed either of numerous smaller graphite cuboids with smooth surfaces or graphite flakes radiating from a common

center. The graphite aggregates showing almost a perfect cubic morphology have been recognized exclusively in the cliftonite-bearing samples from the Ozerskaya mountain intrusion. In contrast to the results obtained in experimental studies of cast iron [107,111,113], the presence of sulfur and oxygen (or sulphides, oxides, silicates) in natural systems does not preclude the crystallization of graphite cuboids. The findings of graphite cuboids in a granite pegmatite (Estes Quarry), which has never been subducted to the diamond stability field, as well as in the diamond-bearing metamorphic rocks indicate that the formation of graphite cuboids may occur in a wide range of PT conditions. The origin of cuboidal graphite is therefore assumed to be unrelated to the partial or complete diamond-graphitization processes, but is attributed instead to graphite precipitation from fluid/melt. The rarity of traces of the spiral growth mechanism on the basal plane of graphite crystals is likely due to their fast crystallization from supersaturated carbon-bearing fluid/melt.

**Author Contributions:** A.V.K. and J.A.J. designed the concept of the manuscript, A.V.K., O.V.R. and J.A.J. performed the SEM examination, A.V.K. and O.V.R. carried out the Raman studies, D.S.M. determined the carbon isotope composition of the Beni Bousera samples. All authors contributed equally to the sample selection/preparation and image processing, A.V.K., O.V.R. and D.I.R. analyzed the data, and A.V.K. wrote the paper with input from all coauthors.

**Funding:** This study was carried out within the IGM SB RAS state assignment project supervised by the Ministry of Science and Higher Education of the Russian Federation. The financial support from the RFBR grants 18-05-00643 and 18-35-20072 is appreciated.

**Acknowledgments:** The authors are grateful to Fabio Carmelo Manuella and two anonymous reviewers for the valuable comments that helped to improve the manuscript.

**Conflicts of Interest:** The authors declare no conflict of interest.

## References

1. Langenhorst, F.; Campione, M. Ideal and real structures of carbon forms with some remarks on the geological significance. *J. Geol. Soc.* **2018**. [[CrossRef](#)]
2. Smith, D.C.; Dobrzhinetskaya, L.F.; Godard, G.; Green, H.W. Diamond–lonsdaleite–graphite relations examined by Raman mapping of carbon microinclusions inside zircon at Kumdy Kol, Kokchetav, Kazakhstan: evidence of the metamictization of diamond. In *Ultrahigh-Pressure Metamorphism*; Elsevier: Amsterdam, The Netherlands, 2011; pp. 43–75.
3. Hanneman, R.; Strong, H.; Bundy, F. Hexagonal diamonds in meteorites: Implications. *Science* **1967**, *155*, 995–997. [[CrossRef](#)] [[PubMed](#)]
4. Vdovykin, G.P. Forms of carbon in the new Haverö ureilite of Finland. *Meteoritics* **1972**, *7*, 547–552. [[CrossRef](#)]
5. Masaitis, V.L.; Futergendler, S.I.; Gnevushev, M.A. Diamonds in impactites of the Popigai meteorite crater. *All-Union Mineral. Soc. Proc.* **1972**, *1*, 108–112.
6. Masaitis, V.L.; Shafranovskii, G.I.; Ezerskii, V.A.; Reshetniak, N.B. Impact diamonds in ureilites and impactites. *Meteoritika* **1990**, *49*, 180–196.
7. Vishnevsky, S.A.; Pal'chik, N.A. Graphite in the rocks of Popigai structure: Destruction and transformation to other phases of the carbon system. *Geol. Geofiz.* **1975**, *1*, 67–75. (In Russian)
8. Marakushev, A.A. Geological position, geochemistry, and thermodynamics of diamondiferous impactogenesis. *Mosc. Univ. Geol. Bull.* **1995**, *50*, 1–19. (In Russian)
9. Gurov, Y.P.; Gurova, Y.P.; Sokur, T.M. Impact diamonds in rocks of Zapadnaya astrobleme. *Miner. Resur. Ukr.* **1999**, *3*, 30–32. (In Russian)
10. El Goresy, A.; Dubrovinsky, L.S.; Gillet, P.; Mostefaoui, S.; Graup, G.; Drakopoulos, M.; Simionovici, A.S.; Swamy, V.; Masaitis, V.L. A new natural, super-hard, transparent polymorph of carbon from the Popigai impact crater, Russia. *Comptes Rendus Geosci.* **2003**, *335*, 889–898. [[CrossRef](#)]
11. Rubin, A.E. Shock, post-shock annealing, and post-annealing shock in ureilites. *Meteorit. Planet. Sci.* **2006**, *41*, 125–133. [[CrossRef](#)]
12. Kennett, D.J.; Kennett, J.P.; West, A.; West, G.J.; Bunch, T.E.; Culleton, B.J.; Erlandson, J.M.; Hee, S.S.Q.; Johnson, J.R.; Mercer, C.; et al. Shock-synthesized hexagonal diamonds in Younger Dryas boundary sediments. *Proc. Natl. Acad. Sci. USA* **2009**, *106*, 12623–12628. [[CrossRef](#)] [[PubMed](#)]



13. Godard, G.; Frezzotti, M.L.; Palmeri, R.; Smith, D.C. Origin of high-pressure disordered metastable phases (lonsdaleite and incipiently amorphized quartz) in metamorphic rocks: Geodynamic shock or crystal-scale overpressure? In *Ultrahigh-Pressure Metamorphism*; Elsevier: Amsterdam, The Netherlands, 2011; pp. 125–148.
14. Golovnya, S.V.; Khvostova, V.P.; Makarov, E.S. Hexagonal modification of diamond (lonsdaleite) in the eclogites of metamorphic complexes. *Geochem. Int.* **1977**, *14*, 82–84.
15. Kuzovkov, G.N. Maksyutov complex in the southern Urals a cornerstone of Urals geodynamics. *Otechestvennaya Geol.* **2001**, 58–59. (In Russian)
16. Dubinchuk, V.T.; Simakov, S.K.; Pechnikov, V.A. Lonsdaleite in diamond-bearing metamorphic rocks of the Kokchetav Massif. *Dokl. Earth Sci.* **2010**, *430*, 40–42. [[CrossRef](#)]
17. Jones, A.P.; McMillan, P.F.; Salzmann, C.G.; Alvaro, M.; Nestola, F.; Prencipe, M.; Dobson, D.; Hazael, R.; Moore, M. Structural characterization of natural diamond shocked to 60 GPa; implications for Earth and planetary systems. *Lithos* **2016**, *265*, 214–221. [[CrossRef](#)]
18. Mikhailenko, D.S.; Korsakov, A.V.; Zelenovskiy, P.S.; Golovin, A.V. Graphite-diamond relations in mantle rocks: Evidence from an eclogitic xenolith from the Udachnaya kimberlite (Siberian Craton). *Am. Mineral.* **2016**, *101*, 2155–2167. [[CrossRef](#)]
19. Bulanov, G.P. The formation of diamonds. *J. Geochem. Explor.* **1995**, *53*, 1–23. [[CrossRef](#)]
20. Glinnemann, J.; Kusaka, K.; Harris, J.W. Oriented graphite single-crystal inclusions in diamond. *Z. Krist. Cryst. Mater.* **2003**, *218*, 733–739. [[CrossRef](#)]
21. Nasdala, L.; Hofmeister, W.; Harris, J.W.; Glinnemann, J. Growth zoning and strain patterns inside diamond crystals as revealed by Raman maps. *Am. Mineral.* **2005**, *90*, 745–748. [[CrossRef](#)]
22. Korsakov, A.V.; Perraki, M.; Zedgenizov, D.A.; Bindi, L.; Vandenabeele, P.; Suzuki, A.; Kagi, H. Diamond-Graphite Relationships in Ultrahigh-pressure Metamorphic Rocks from the Kokchetav Massif, Northern Kazakhstan. *J. Petrol.* **2010**, *51*, 763–783. [[CrossRef](#)]
23. Perraki, M.; Proyer, A.; Mposkos, E.; Kaindl, R.; Hoinkes, G. Raman micro-spectroscopy on diamond, graphite and other carbon polymorphs from the ultrahigh-pressure metamorphic Kimi Complex of the Rhodope Metamorphic Province, NE Greece. *Earth Planet. Sci. Lett.* **2006**, *241*, 672–685. [[CrossRef](#)]
24. Perraki, M.; Korsakov, A.V.; Smith, D.C.; Mposkos, E. Raman spectroscopic and microscopic criteria for the distinction of microdiamonds in ultrahigh-pressure metamorphic rocks from diamond in sample preparation materials. *Am. Mineral.* **2009**, *94*, 546–556. [[CrossRef](#)]
25. Ryabov, V.V.; Lapkovsky, A.A. Native iron (–platinum) ores from the Siberian Platform trap intrusions. *Aust. J. Earth Sci.* **2010**, *57*, 707–736. [[CrossRef](#)]
26. Doroshkevich, A.G.; Wall, F.; Ripp, G.S. Magmatic graphite in dolomite carbonatite at Pogranichnoe, North Transbaikalia, Russia. *Contrib. Mineral. Petrol.* **2007**, *153*, 339–353. [[CrossRef](#)]
27. Pasteris, J.D. Occurrence of graphite in serpentinized olivines in kimberlite. *Geology* **1981**, *9*, 356–359. [[CrossRef](#)]
28. Jedwab, J.; Boulègue, J. Graphite crystals in hydrothermal vents. *Nature* **1984**, *310*, 41. [[CrossRef](#)]
29. Luque, F.J.; Pasteris, J.D.; Wopenka, B.; Rodas, M.; Barrenechea, J.F. Natural fluid-deposited graphite: Mineralogical characteristics and mechanisms of formation. *Am. J. Sci.* **1998**, *298*, 471–498. [[CrossRef](#)]
30. Luque, F.J.; Ortega, L.; Barrenechea, J.F.; Millward, D.; Beyssac, O.; Huizenga, J.M. Deposition of highly crystalline graphite from moderate-temperature fluids. *Geology* **2009**, *37*, 275–278. [[CrossRef](#)]
31. Weis, P.L. Graphite skeleton crystals—A newly recognized morphology of crystalline carbon in metasedimentary rocks. *Geology* **1980**, *8*, 296–297. [[CrossRef](#)]
32. Jaszczak, J.A. Unusual Graphite Crystals: From the Lime Crest Quarry, Sparta, New Jersey. *Rocks Miner.* **1997**, *72*, 330–334. [[CrossRef](#)]
33. Jaszczak, J.A.; Trinchillo, D. Miracle at Merelani A Remarkable Occurrence of Graphite, Diopside, and Associated Minerals from the Karo Mine, Block D, Merelani Hills, Arusha Region, Tanzania. *Rocks Miner.* **2013**, *88*, 154–165. [[CrossRef](#)]
34. Jaszczak, J.A.; Robinson, G.W.; Dimovski, S.; Gogotsi, Y. Naturally occurring graphite cones. *Carbon* **2003**, *41*, 2085–2092. [[CrossRef](#)]
35. Slodkevich, V.V. Polycrystalline aggregates of octahedral-shaped graphite. *Dokl. Akad. Nauk SSSR* **1980**, *253*, 697–700. (In Russian)
36. Slodkevich, V.V. Graphite paramorphs after diamond. *Proc. Russ. Mineral. Soc.* **1982**, *111*, 13–33. (In Russian) [[CrossRef](#)]

37. Korsakov, A.V.; Theunissen, K.; Smirnova, L.V. Intergranular diamonds derived from partial melting of crustal rocks at ultrahigh-pressure metamorphic conditions. *Terra Nova* **2004**, *16*, 146–151. [[CrossRef](#)]
38. Korsakov, A.V.; Shatsky, V.S. Origin of graphite-coated diamonds from the UHP metamorphic rocks. *Dokl. Earth Sci.* **2004**, *399*, 1160–1163.
39. Massonne, H.-J.; Bernhardt, H.J.; Dettmar, D.; Kessler, E.; Medenbach, O.; Westphal, T. Simple identification and quantification of microdiamonds in rock thin-sections. *Eur. J. Mineral.* **1998**, *10*, 497–504. [[CrossRef](#)]
40. Katayama, I.; Zayachkovsky, A.A.; Maruyama, S. Prograde P-T records from inclusions in zircons from ultrahigh-pressure rocks of the Kokchetav massif, northern Kazakhstan. *Island Arc* **2000**, *9*, 417–427. [[CrossRef](#)]
41. Ogasawara, Y.; Ohta, M.; Fukasawa, K.; Katayama, I.; Maruyama, S. Diamond-bearing and diamond-free metacarbonate rocks from Kumdy-Kol in the Kokchetav massif, northern Kazakhstan. *Island Arc* **2000**, *9*, 400–416. [[CrossRef](#)]
42. Zhu, Y.F.; Ogasawara, Y. Carbon recycled into the deep Earth: Evidenced by dolomite dissociation in subduction-zone rocks. *Geology* **2002**, *30*, 947–950. [[CrossRef](#)]
43. Dobrzhinetskaya, L.F.; Wirth, R.; Rhede, D.; Liu, Z.; Green, H.W. Phlogopite and quartz lamellae in diamond-bearing diopside from marbles of the Kokchetav massif, Kazakhstan: Exsolution or replacement reaction? *J. Metamorph. Geol.* **2009**, *27*, 607–620. [[CrossRef](#)]
44. Naemura, K.; Ikuta, D.; Kagi, H.; Otake, S.; Ueda, T.; Ohi, S.; Kobayashi, T.; Svojtka, M.; Hirajima, T. Diamond and other possible ultradeep evidence discovered in the orogenic spinel-garnet peridotite from the Moldanubian Zone of the Bohemian Massif, Czech Republic. In *Ultrahigh-Pressure Metamorphism 25 Years after Discovery of Coesite and Diamond*; Dobrzhinetskaya, L.F., Faryad, S.W., Wallis, S., Cuthbert, S., Eds.; Elsevier: Amsterdam, The Netherlands, 2011; pp. 77–105.
45. Janák, M.; Krogh Ravna, E.; Kullerød, K.; Yoshida, K.; Milovský, R.; Hirajima, T. Discovery of diamond in the Tromsø Nappe, Scandinavian Caledonides (N. Norway). *J. Metamorph. Geol.* **2013**, *31*, 691–703. [[CrossRef](#)]
46. El Goresy, A. Mineralbestand und Strukturen der Graphit- und Sulfideinschlüsse in Eisenmeteoriten. *Geochim. Cosmochim. Acta* **1965**, *29*, 1131–1151. [[CrossRef](#)]
47. Brett, R.; Higgins, G.T. Cliftonite: A proposed origin, and its bearing on the origin of diamonds in meteorites. *Geochim. Cosmochim. Acta* **1969**, *33*, 1473–1484. [[CrossRef](#)]
48. Korsakov, A.V.; Zhimulev, E.I.; Mikhailenko, D.S.; Demin, S.P.; Kozmenko, O.A. Graphite pseudomorphs after diamonds: An experimental study of graphite morphology and the role of H<sub>2</sub>O in the graphitisation process. *Lithos* **2015**, *236–237*, 16–26. [[CrossRef](#)]
49. Fedortchouk, Y.; Manghnani, M.H.; Hushur, A.; Shiryayev, A.; Nestola, F. An atomic force microscopy study of diamond dissolution features: The effect of H<sub>2</sub>O and CO<sub>2</sub> in the fluid on diamond morphology. *Am. Mineral.* **2011**, *96*, 1768–1775. [[CrossRef](#)]
50. Khokhryakov, A.F.; Pal'yanov, Y.N. The evolution of diamond morphology in the process of dissolution: Experimental data. *Am. Mineral.* **2007**, *92*, 909–917. [[CrossRef](#)]
51. Sokol, A.G.; Pal'yanov, Y.N.; Pal'yanova, G.A.; Khokhryakov, A.F.; Borzdov, Y.M. Diamond and graphite crystallization from C-O-H fluids. *Diam. Relat. Mater.* **2001**, *10*, 2131–2136. [[CrossRef](#)]
52. Yamaoka, S.; Kumar, M.D.S.; Kanda, H.; Akaishi, M. Thermal decomposition of glucose and diamond formation under diamond-stable high pressure-high temperature conditions. *Diam. Relat. Mater.* **2002**, *11*, 118–124. [[CrossRef](#)]
53. Harley, S.L. On the occurrence and characterization of ultrahigh-temperature crustal metamorphism. *Geol. Soc. Lond. Spec. Publ.* **1998**, *138*, 81–107. [[CrossRef](#)]
54. Zheng, Y.F.; Chen, R.X. Regional metamorphism at extreme conditions: Implications for orogeny at convergent plate margins. *J. Asian Earth Sci.* **2017**, *145*, 46–73. [[CrossRef](#)]
55. Okamoto, K.; Liou, J.G.; Ogasawara, Y. Petrology of the diamond-grade eclogite in the Kokchetav Massif, northern Kazakhstan. *Island Arc* **2000**, *9*, 379–399. [[CrossRef](#)]
56. Ogasawara, Y.; Fukasawa, K.; Maruyama, S. Coesite exsolution from supersilicic titanite in UHP marble from the Kokchetav massif, northern Kazakhstan. *Am. Mineral.* **2002**, *87*, 454–461. [[CrossRef](#)]
57. Massonne, H.-J. A comparison of the evolution of diamondiferous quartz-rich rocks from the Saxonian Erzgebirge and the Kokchetav massif: Are so-called diamondiferous gneisses magmatic rocks? *Earth Planet. Sci. Lett.* **2003**, *216*, 347–364. [[CrossRef](#)]



58. Mikhno, A.O.; Korsakov, A.V. K<sub>2</sub>O prograde zoning pattern in clinopyroxene from the Kokchetav diamond-grade metamorphic rocks: Missing part of metamorphic history and location of second critical end point for calc-silicate system. *Gondwana Res.* **2013**, *23*, 920–930. [[CrossRef](#)]
59. De Corte, K. Study of Microdiamonds from UHP Metamorphic Rocks of the Kokchetav Massif (Northern Kazakhstan): Characterisation and Genesis. Ph.D. Thesis, Ghent University, Ghent, Belgium, 2000.
60. Reutsky, V.N.; Borzdov, Y.M.; Palyanov, Y.N. Effect of diamond growth rate on carbon isotope fractionation in Fe–Ni–C system. *Diam. Relat. Mater.* **2012**, *21*, 7–10. [[CrossRef](#)]
61. Stepanov, A.S.; Rubatto, D.; Hermann, J.; Korsakov, A.V. Associated and contrasting P–T paths within the Barchi-Kol UHP terrain (Kokchetav Complex): Implications for subduction and exhumation of continental crust. *Am. Mineral.* **2016**, *101*, 788–807. [[CrossRef](#)]
62. Beane, R.J.; Liou, J.G.; Coleman, R.G.; Leech, M.L. Mineral assemblages and retrograde PT path for high- to ultrahigh-pressure metamorphism in the lower unit of the Maksyutov Complex, Southern Ural Mountains, Russia. *Island Arc* **1995**, *4*, 254–266. [[CrossRef](#)]
63. El Atrassi, F.; Brunet, F.; Bouybaouene, M.; Chopin, C.; Chazot, G. Melting textures and microdiamonds preserved in graphite pseudomorphs from the Beni Bousera peridotite massif, Morocco. *Eur. J. Mineral.* **2011**, *23*, 157–168. [[CrossRef](#)]
64. Rozen, O.M.; Zorin, Y.M.; Zayachkovsky, A.A. A find of diamond linked with eclogites of the Precambrian Kokchetav massif. *Dokl. Akad. Nauk SSSR* **1972**, *203*, 674–676. (In Russian)
65. Letnikov, F.A. Formation of diamonds in deep-seated tectonic zones. *Dokl. Akad. Nauk SSSR* **1983**, *271*, 433–435. (In Russian)
66. Sobolev, N.V.; Shatsky, V.S. Diamond inclusions in garnets from metamorphic rocks: A new environment for diamond formation. *Nature* **1990**, *343*, 742–746. [[CrossRef](#)]
67. Schertl, H.P.; Sobolev, N. The Kokchetav Massif, Kazakhstan: “Type locality” of diamond-bearing UHP metamorphic rocks. *J. Asian Earth Sci.* **2013**, *63*, 5–38. [[CrossRef](#)]
68. De Corte, K.; Korsakov, A.; Taylor, W.R.; Cartigny, P.; Ader, M.; De Paepe, P. Diamond growth during ultrahigh-pressure metamorphism of the Kokchetav massif, northern Kazakhstan. *Island Arc* **2000**, *9*, 284–303. [[CrossRef](#)]
69. Dobrzhinetskaya, L.F.; Braun, T.V.; Sheshkel, G.G.; Podkuiko, Y.A. Geology and structure of diamond-bearing rocks of the Kokchetav massif, Kazakhstan. *Tectonophysics* **1994**, *233*, 293–313. [[CrossRef](#)]
70. Dobretsov, N.L.; Sobolev, N.V.; Shatsky, V.S.; Coleman, R.G.; Ernst, W.G. Geotectonic evolution of diamondiferous paragneisses of the Kokchetav complex, Northern Kazakhstan—The geologic enigma of ultrahigh-pressure crustal rocks within Phanerozoic foldbelt. *Island Arc* **1995**, *4*, 267–279. [[CrossRef](#)]
71. Shatsky, V.S.; Sobolev, N.V.; Vavilov, M.A. *Ultra-High Pressure Metamorphism*; Cambridge University Press: Cambridge, UK, 1995; pp. 427–455.
72. Lavrova, L.D.; Pechnikov, V.A.; Pleshakov, M.A.; Nadajdina, E.D.; Shukolyukov, Y.A. *A New Genetic Type of Diamond Deposit*; Scientific World: Moscow, Russia, 1999.
73. Lavrova, L.D.; Pechnikov, V.A.; Petrova, M.A.; Zayachkovsky, A.A. Geology of diamondiferous Barchi-Kol area. *Otechestvennaya Geol.* **1996**, 20–27.
74. Korsakov, A.V.; Shatsky, V.S.; Sobolev, N.V. The first finding of coesite in eclogites of the Kokchetav massif. *Dokl. Akad. Nauk SSSR* **1998**, *360*, 77–81.
75. Korsakov, A.V.; Shatsky, V.S.; Sobolev, N.V.; Zayachkovsky, A.A. Garnet-biotite-clinozoisite gneisses: A new type of diamondiferous metamorphic rocks of the Kokchetav massif. *Eur. J. Mineral.* **2002**, *14*, 915–929. [[CrossRef](#)]
76. Korsakov, A.V.; Toporski, J.; Dieing, T.; Yang, J.; Zelenovskiy, P. Internal diamond morphology: Raman imaging of metamorphic diamonds. *J. Raman Spectrosc.* **2015**, *46*, 880–888. [[CrossRef](#)]
77. Stepanov, A.S.; Hermann, J.; Korsakov, A.V.; Rubatto, D. Geochemistry of ultrahigh-pressure anatexis: Fractionation of elements in the Kokchetav gneisses during melting at diamond-facies conditions. *Contrib. Mineral. Petrol.* **2014**, *167*, 1–25. [[CrossRef](#)]
78. Stepanov, A.S.; Hermann, J.; Rubatto, D.; Korsakov, A.V.; Danyushevsky, L.V. Melting History of an Ultrahigh-pressure Paragneiss Revealed by Multiphase Solid Inclusions in Garnet, Kokchetav Massif, Kazakhstan. *J. Petrol.* **2016**, *57*, 1531–1554. [[CrossRef](#)]

79. Mikhno, A.O.; Musiyachenko, K.A.; Shchepetova, O.V.; Korsakov, A.V.; Rashchenko, S.V. CO<sub>2</sub>-bearing fluid inclusions associated with diamonds in zircon from the UHP Kokchetav gneisses. *J. Raman Spectrosc.* **2017**, *48*, 1566–1573. [\[CrossRef\]](#)
80. Shchepetova, O.V.; Korsakov, A.; Mikhailenko, D.; Zelenovskiy, P.; Shur, V.; Ohfuji, H. Forbidden mineral assemblage coesite-disordered graphite in diamond-bearing kyanite gneisses (Kokchetav Massif). *J. Raman Spectrosc.* **2017**, *48*, 1606–1612. [\[CrossRef\]](#)
81. Pechnikov, V.A.; Kaminsky, F.V. Diamond potential of metamorphic rocks in the Kokchetav Massif, northern Kazakhstan. *Eur. J. Mineral.* **2008**, *20*, 395–413. [\[CrossRef\]](#)
82. De Corte, K.; Trautman, R.; Griffin, B.; De Paepe, P. Internal morphology of microdiamonds from UHPM rocks of the Kokchetav Massif. In *The Diamond-Bearing Kokchetav Massif*; Universal Academy Press: Tokyo, Japan, 2002; pp. 103–114.
83. Korsakov, A.V.; Vandenabeele, P.; Theunissen, K. Discrimination of metamorphic diamond populations by Raman spectroscopy (Kokchetav, Kazakhstan). *Spectrochim. Acta Part A* **2005**, *61*, 2378–2385. [\[CrossRef\]](#) [\[PubMed\]](#)
84. Yoshioka, N.; Ogasawara, Y. Cathodoluminescence of microdiamond in dolomite marble from the Kokchetav Massif—Additional evidence for two-stage growth of diamond. *Int. Geol. Rev.* **2005**, *47*, 703–715. [\[CrossRef\]](#)
85. Schertl, H.P.; Sobolev, N.V.; Neuser, R.D.; Shatsky, V.S. HP-metamorphic rocks from Dora Maira/Western Alps and Kokchetav/Kazakhstan: New insights using cathodoluminescence petrography. *Eur. J. Mineral.* **2004**, *16*, 49–57. [\[CrossRef\]](#)
86. Mikhno, A.O.; Korsakov, A.V. Carbonate, silicate, and sulfide melts: Heterogeneity of the UHP mineral-forming media in calc-silicate rocks from the Kokchetav massif. *Russ. Geol. Geophys.* **2015**, *56*, 81–99. [\[CrossRef\]](#)
87. Ishida, H.; Ogasawara, Y.; Ohsumi, K.; Saito, A. Two stage growth of microdiamond in UHP dolomite marble from Kokchetav Massif, Kazakhstan. *J. Metamorph. Geol.* **2003**, *21*, 515–522. [\[CrossRef\]](#)
88. Shatsky, V.S.; Rylov, G.M.; Efimova, E.S.; Corte, K.D.; Sobolev, N.V. Morphology and real structure of microdiamonds from metamorphic rocks of the Kokchetav massif, kimberlites, and alluvial placers. *Geol. Geofiz.* **1998**, *39*, 942–956. (In Russian)
89. Korsakov, A.V. Application of Raman Imaging in UHPM Research. In *Confocal Raman Microscopy*; Springer Series in Surface Sciences; Springer: Cham, Switzerland, 2018; pp. 237–258.
90. Rakovan, J.; Jaszczak, J.A. Multiple length scale growth spirals on metamorphic graphite {001} surfaces studied by atomic force microscopy. *Am. Mineral.* **2002**, *87*, 17–24. [\[CrossRef\]](#)
91. Thompson, W.B.; Bearss, G.T.; Falster, A.U.; Simmons, W.B.; Nizamoff, J.W. The Estes Quarry, Cumberland County, Maine: A New Pegmatite Mineral Locality. *Rocks Miner.* **2000**, *75*, 408–418. [\[CrossRef\]](#)
92. Dobretsov, N.L.; Shatsky, V.S.; Coleman, R.G.; Lennykh, V.I.; Valizer, P.M.; Liou, J.; Zhang, R.; Beane, R.J. Tectonic Setting and Petrology of Ultrahigh-Pressure Metamorphic Rocks in the Maksyutov Complex, Ural Mountains, Russia. *Int. Geol. Rev.* **1996**, *38*, 136–160. [\[CrossRef\]](#)
93. Chesnokov, B.V.; Popov, V.A. Increasing volume of quartz grains in eclogites of the South Urals. *Dokl. Akad. Nauk SSSR* **1965**, *162*, 176–178.
94. Leech, M.L.; Ernst, W.G. Graphite pseudomorphs after diamond? A carbon isotope and spectroscopic study of graphite cuboids from the Maksyutov Complex, south Ural Mountains, Russia. *Geochim. Cosmochim. Acta* **1998**, *62*, 2143–2154. [\[CrossRef\]](#)
95. Pearson, D.G.; Davies, G.R.; Nixon, P.H. Geochemical constraints on the petrogenesis of diamond facies pyroxenites from the Beni Bousera peridotite massif, North Morocco. *J. Petrol.* **1993**, *34*, 125–172. [\[CrossRef\]](#)
96. Pearson, D.G.; Davies, G.R.; Nixon, P.H.; Milledge, H.J. Graphitized diamonds from a peridotite massif in Morocco and implications for anomalous diamond occurrences. *Nature* **1989**, *338*, 60–62. [\[CrossRef\]](#)
97. Pearson, D.G.; Davies, G.R.; Nixon, P.H.; Matthey, D.P. A carbon isotope study of diamond facies pyroxenites and associated rocks from the Beni Bousera Peridotite, North Morocco. *J. Petrol.* **1991**, *2*, 175–189. [\[CrossRef\]](#)
98. Levashov, V.K.; Oleinikov, B.V. Earth cliftonite in the association with native iron of gabbro-dolerites of the Ozernaia mountain (Siberian Platform). *Dokl. Akad. Nauk SSSR* **1984**, *278*, 719–722.
99. Ryabov, V.V.; Pavlov, A.L.; Lopatin, G.G. *Native Iron of the Siberian Traps*; Nauka: Novosibirsk, Russia, 1985.
100. Tuinstra, F.; Koenig, J.L. Raman spectrum of graphite. *J. Chem. Phys.* **1970**, *53*, 1126–1130. [\[CrossRef\]](#)
101. Nemanich, R.J.; Solin, S.A. First- and second-order Raman scattering from finite-size crystals of graphite. *Phys. Rev. B* **1979**, *20*, 392–401. [\[CrossRef\]](#)

102. Wopenka, B.; Pasteris, J.D. Structural characterization of kerogens to granulite-facies graphite: Applicability of Raman microprobe spectroscopy. *Am. Mineral.* **1993**, *78*, 533–557.
103. Ferrari, A.C.; Robertson, J. Interpretation of Raman spectra of disordered and amorphous carbon. *Phys. Rev. B* **2000**, *61*, 14095–14107. [[CrossRef](#)]
104. Beyssac, O.; Rouzaud, J.N.; Goffe, B.; Brunet, F.; Chopin, C. Graphitization in high-pressure, low-temperature metamorphic gradient: A HRTEM and Raman microspectroscopy study. *Contrib. Mineral. Petrol.* **2002**, *143*, 19–31. [[CrossRef](#)]
105. Beyssac, O.; Goffe, B.; Chopin, C.; Rouzaud, J.N. Raman spectra of carbonaceous material from metasediments: A new geothermometer. *J. Metamorph. Geol.* **2002**, *20*, 859–871. [[CrossRef](#)]
106. Perchuk, L.L.; Safonov, O.G.; Yapaskurt, V.O.; Barton, J.M., Jr. Crystal-melt equilibria involving potassium-bearing clinopyroxene as indicator of mantle-derived ultrahigh-potassic liquids: An analytical review. *Lithos* **2002**, *60*, 89–111. [[CrossRef](#)]
107. Johnson, W.; Smartt, H. The role of interphase boundary adsorption in the formation of spheroidal graphite in cast iron. *Metall. Trans. A* **1977**, *8*, 553–565. [[CrossRef](#)]
108. Jaszczak, J.A. Graphite: Flat, fibrous and spherical. In *Mesomolecules*; Springer: Dordrecht, The Nederland, 1995; pp. 161–180.
109. Double, D.D.; Hellawell, A. The structure of flake graphite in Ni-C eutectic alloy. *Acta Metall.* **1969**, *17*, 1071–1083. [[CrossRef](#)]
110. Double, D.D.; Hellawell, A. Cone-helix growth forms of graphite. *Acta Metall.* **1974**, *22*, 481–487. [[CrossRef](#)]
111. Double, D.D.; Hellawell, A. The nucleation and growth of graphite—The modification of cast iron. *Acta Metall. Mater.* **1995**, *43*, 2435–2442. [[CrossRef](#)]
112. Sadocha, J.P.; Gruzleski, J.E. The mechanism of graphite spheroid formation in pure Fe–C–Si alloys, In *The Metallurgy of Cast Iron*; Lux, B., Minkoff, I., Mollard, F., Eds.; Georgi Publishing Co.: St Saphorin, Switzerland, 1975; pp. 443–459.
113. Stefanescu, D.M.; Alonso, G.; Larrañaga, P.; De la Fuente, E.; Suarez, R. On the crystallization of graphite from liquid iron–carbon–silicon melts. *Acta Mater.* **2016**, *107*, 102–126. [[CrossRef](#)]
114. Ugarte, D. Curling and closure of graphitic networks under electron-beam irradiation. *Nature* **1992**, *359*, 707. [[CrossRef](#)] [[PubMed](#)]
115. Miao, B.; Fang, K.; Bian, W.; Liu, G. On the microstructure of graphite spherulites in cast irons by TEM and HREM. *Acta Metall. Mater.* **1990**, *38*, 2167–2174. [[CrossRef](#)]
116. Jehlička, J.; Frank, O.; Hamplová, V.; Pokorná, Z.; Juha, L.; Boháček, Z.; Weishauptová, Z. Low extraction recovery of fullerene from carbonaceous geological materials spiked with C60. *Carbon* **2005**, *43*, 1909–1917. [[CrossRef](#)]
117. Daly, T.K.; Buseck, P.R.; Williams, P.; Lewis, C.F. Fullerenes from a fulgurite. *Science* **1993**, *259*, 1599–1601. [[CrossRef](#)] [[PubMed](#)]
118. Becker, L.; Bada, J.L.; Winans, R.E.; Hunt, J.E.; Bunch, T.E.; French, B.M. Fullerenes in the 1.85-billion-year-old Sudbury impact structure. *Science* **1994**, *265*, 642–645. [[CrossRef](#)]
119. Jehlička, J.; Svatoš, A.; Frank, O.; Uhlik, F. Evidence for fullerenes in solid bitumen from pillow lavas of Proterozoic age from Mitov (Bohemian Massif, Czech Republic). *Geochim. Cosmochim. Acta* **2003**, *67*, 1495–1506. [[CrossRef](#)]
120. Cruz, M.D.R. Are nanotubes and carbon nanostructures the precursors of coexisting graphite and micro-diamonds in UHP rocks? *Diam. Relat. Mater.* **2013**, *40*, 24–31. [[CrossRef](#)]
121. Cruz, M.D.R. Characterization of natural carbon particles formed at low temperature UHP conditions. *Diam. Relat. Mater.* **2016**, *61*, 76–90. [[CrossRef](#)]
122. Massonne, H.-J. Wealth of P–T–t information in medium-high grade metapelites: Example from the Jubrique Unit of the Betic Cordillera, S Spain. *Lithos* **2014**, *208*, 137–157. [[CrossRef](#)]
123. Grenville-Wells, H. The graphitization of diamond and the nature of cliftonite. (With Plate XXVI). *Mineral. Mag. J. Mineral. Soc.* **1952**, *29*, 803–816. [[CrossRef](#)]
124. Oleinikov, B.V. *Geochemistry and Ore Genesis of Platform Basic*; Nauka Publisher: Novosibirsk, Russia, 1979.
125. Oleinikov, B.V.; Okrugin, A.V.; Tomshin, M.D.; Levashov, V.K.; Varganov, A.S.; Kopylova, A.G.; Pankov, V.Y. *Native Metal Formation in Platform Basic Rocks*; Yakutian Scientific Center, Siberian Branch of the Russian Academy of Sciences: Yakutsk, Russia, 1985.



126. Hwang, S.L.; Shen, P.; Chu, H.T.; Yui, T.F.; Lin, C.C. Genesis of microdiamonds from melt and associated multiphase inclusions in garnet of ultrahigh-pressure gneiss from Erzgebirge, Germany. *Earth Planet. Sci. Lett.* **2001**, *188*, 9–15. [\[CrossRef\]](#)
127. Stöckhert, B.; Duyster, J.; Trepmann, C.; Massonne, H.-J. Microdiamond daughter crystals precipitated from supercritical C-O-H fluids included in garnet, Erzgebirge, Germany. *Geology* **2001**, *29*, 391–394. [\[CrossRef\]](#)
128. Korsakov, A.V.; Hermann, J. Silicate and carbonate melt inclusions associated with diamonds in deeply subducted carbonate rocks. *Earth Planet. Sci. Lett.* **2006**, *241*, 104–118. [\[CrossRef\]](#)
129. Sokol, A.G.; Pal'yanov, Y.N. Diamond formation in the system MgO–SiO<sub>2</sub>–H<sub>2</sub>O–C at 7.5 GPa and 1600 C. *Contrib. Mineral. Petrol.* **2008**, *155*, 33–43. [\[CrossRef\]](#)
130. Manuella, F.C. Can nanodiamonds grow in serpentinite-hosted hydrothermal systems? A theoretical modelling study. *Mineral. Mag.* **2013**, *77*, 3163–3174. [\[CrossRef\]](#)
131. Manuella, F.C.; Scribano, V.; Carbone, S. Abyssal serpentinites as gigantic factories of marine salts and oil. *Mar. Pet. Geol.* **2018**, *92*, 1041–1055. [\[CrossRef\]](#)
132. Hwang, S.L.; Shen, P.; Chu, H.T.; Yui, T.F.; Liou, J.G.; Sobolev, N.V.; Shatsky, V.S. Crust-derived potassic fluid in metamorphic microdiamond. *Earth Planet. Sci. Lett.* **2005**, *231*, 295–306. [\[CrossRef\]](#)
133. Hwang, S.L.; Chu, H.T.; Yui, T.F.; Shen, P.; Schertl, H.P.; Liou, J.G.; Sobolev, N.V. Nanometer-size P/K-rich silica glass (former melt) inclusions in microdiamond from the gneisses of Kokchetav and Erzgebirge massifs: Diversified characteristics of the formation media of metamorphic microdiamond in UHP rocks due to host-rock buffering. *Earth Planet. Sci. Lett.* **2006**, *243*, 94–106. [\[CrossRef\]](#)
134. Dobrzhinetskaya, L.F.; Wirth, R.; Green II, H.W. Direct observation and analysis of a trapped COH fluid growth medium in metamorphic diamond. *Terra Nova* **2005**, *17*, 472–477. [\[CrossRef\]](#)
135. Dobrzhinetskaya, L.F.; Wirth, R.; Green, H.W., II. A look inside of diamond-forming media in deep subduction zones. *Proc. Natl. Acad. Sci. USA* **2007**, *104*, 9128–9132. [\[CrossRef\]](#) [\[PubMed\]](#)
136. Pal'yanov, Y.N.; Sokol, A.G.; Borzdov, Y.M.; Khokhryakov, A.F. Fluid-bearing alkaline carbonate melts as the medium for the formation of diamonds in the Earth's mantle: An experimental study. *Lithos* **2002**, *60*, 145–159. [\[CrossRef\]](#)
137. Jaszczak, J.A.; Chamberlain, S.C.; Robinson, G.W. The Graphites of New York: Scientific and Aesthetic Surprises. *Rocks Miner.* **2009**, *84*, 502–519. [\[CrossRef\]](#)
138. Majka, J.; Rosén, A.; Janák, M.; Froitzheim, N.; Klonowska, I.; Manecki, M.; Sasinková, V.; Yoshida, K. Microdiamond discovered in the Seve Nappe (Scandinavian Caledonides) and its exhumation by the “vacuum-cleaner” mechanism. *Geology* **2014**, *42*, 1107–1110. [\[CrossRef\]](#)
139. Davies, G.R.; Nixon, P.H.; Pearson, D.G.; Obata, M. The tectonic implications of graphitised diamonds from the Ronda peridotite massif, S. Spain. *Geology* **1993**, *21*, 471–474. [\[CrossRef\]](#)
140. Orlov, Y.L. *Diamond Morphology*; AS USSR: Moscow, Russia, 1963.
141. Harris, J. Black material on mineral inclusions and in internal fracture planes in diamond. *Contrib. Mineral. Petrol.* **1972**, *35*, 22–33. [\[CrossRef\]](#)
142. Sunagawa, I. *Crystals: Growth, Morphology and Perfection*; Cambridge University Press: Cambridge, UK, 2005.
143. Ragozin, A.L.; Shatsky, V.S.; Rylov, G.M.; Goryainov, S.V. Coesite inclusions in rounded diamonds from placers of the northeastern Siberian Platform. *Dokl. Earth Sci.* **2002**, *384*, 385–389.
144. Ragozin, A.L.; Shatsky, V.S.; Zedgenizov, D.A.; Mityukhin, S.I. Evidence for evolution of diamond crystallization medium in eclogite xenolith from the Udachnaya kimberlite pipe, Yakutia. *Dokl. Earth Sci.* **2006**, *407*, 465–468. [\[CrossRef\]](#)
145. Sobolev, N.V. Coesite as an indicator of ultrahigh pressures in continental lithosphere. *Russ. Geol. Geophys.* **2006**, *47*, 94–104.

